Korean J. Chem. Eng., 32(7), 1388-1404 (2015)
DOI: 10.1007/s11814-014-0329-3

pISSN: 0256-1115
eISSN: 1975-7220

Mass transfer simulation of nanofiltration membranes for electrolyte solutions through generalized Maxwell-Stefan approach

Vahid Hoshyargar, Farzad Fadaei, and Seyed Nezameddin Ashrafizadeh†

Research Laboratory for Advanced Separation Processes, Department of Chemical Engineering, Iran University of Science and Technology, Narmak, Tehran 16846-13114, Iran
(*Received 18 August 2014 • accepted 7 November 2014*)

Abstract−A comprehensive mathematical model is developed for simulation of ion transport through nanofiltration membranes. The model is based on the Maxwell-Stefan approach and takes into account steric, Donnan, and dielectric effects in the transport of mono and divalent ions. Theoretical ion rejection for multi-electrolyte mixtures was obtained by numerically solving the "hindered transport" based on the generalized Maxwell-Stefan equation for the flux of ions. A computer simulation has been developed to predict the transport in the range of nanofiltration, a numerical procedure developed linearization and discretization form of the governing equations, and the finite volume method was employed for the numerical solution of equations. The developed numerical method is capable of solving equations for multicomponent systems of *n* species no matter to what extent the system shows stiffness. The model findings were compared and verified with the experimental data from literature for two systems of Na_2SO_4+NaCl and $MgCl_2$+NaCl. Comparison showed great agreement for different concentrations. As such, the model is capable of predicting the rejection of different ions at various concentrations. The advantage of such a model is saving costs as a result of minimizing the number of required experiments, while it is closer to a realistic situation since the adsorption of ions has been taken into account. Using this model, the flux of permeates and rejections of multi-component liquid feeds can be calculated as a function of membrane properties. This simulation tool attempts to fill in the gap in methods used for predicting nanofiltration and optimization of the performance of charged nanofilters through generalized Maxwell-Stefan (GMS) approach. The application of the current model may weaken the latter gap, which has arisen due to the complexity of the fundamentals of ion transport processes via this approach, and may further facilitate the industrial development of nanofiltration.

Keywords: Nanofiltration, Maxwell-stefan, Membrane, Mass Transfer, Numerical Simulation

INTRODUCTION

Membrane processes are a novel and growing technology which can be applied to a wide range of separation processes. They can be driven by various driving forces such as pressure, temperature, and electric potential. Pressure-driven membrane processes such as reverse osmosis (RO), ultrafiltration and microfiltration use pressure gradient across the membrane in order to transfer species [1]. These well-established membrane processes are very useful in the removal of salts from aqueous solutions, *e.g.*, to produce potable water. Rejection of salts is mainly governed by exclusion and friction with the membrane matrix.

The major disadvantage of RO membranes is that they need high pressures (up to 100 bars) due to the dense structure of RO membranes, while very low fluxes are obtained (typically 100 $kg \cdot m^{-2}h^{-1}$). Therefore, alternative membrane processes have been developed. Much attention has been focused on nanofiltration (NF) as an alternative for ion removal, and some promising instances have been reported [2,3]. Nanofiltration membranes consist of pores which are larger than those in RO membranes and on the order of low molecular weight salts. The salts are rejected by a combination of electrical and dielectrical forces as well as sterical hindrance between ions and membrane. In NF the operational pressure is considerably reduced (about 10 bar) while moderate fluxes are (typically 50 $kg \cdot m^{-2} h^{-1}$) achieved.

The most important factor in membrane separation is the rejection of various components. In addition to membrane properties and molecular size, the rejection depends on process conditions such as the velocity of phases, applied trans-membrane pressure, and feed concentration.

Several studies have focused on the modeling of ion transport through porous media [4-14]. From a scientific to an industrial viewpoint, there is a definite need to develop comprehensive transport models which require minimum adjustable parameters. The first step is the development of a multi-component boundary layer theory for the prediction of polarization layer adjacent to the membrane wall. Some studies have used a film approximation in which the properties do not explicitly depend on the flow field near the membrane. Instead, other studies have used the main mass transfer equation for the concentration polarization layer. Noteworthy, if the diluted solutions are fed to membrane, the boundary layer would not impose major effects on transportation of species.

The second step is prediction of the transport phenomena inside the membrane pores. Modeling of transport through membranes

†To whom correspondence should be addressed.
E-mail: ashrafi@iust.ac.ir

has been the subject of a large number of studies. Multi-component diffusion can be used to describe transport inside the NF membranes. Generalized Maxwell-Stefan equations are the main equations used for the diffusion process in a multi-component system. This formulation is able to describe the diffusion process in the majority of phases (liquid and solid phases) as well as in microporous materials such as NF membranes. The Maxwell-Stefan equations can be solved either analytically (only in special cases) or by numerical methods. Mass transfer is described in terms of intermolecular friction [15]. The generalized Maxwell-Stefan equation (GMS) relates driving forces and intermolecular friction to net diffusion velocities, and hence to mass transfer fluxes [15-17]. The equations include frictional interactions among each set of species (including the membrane).

The common result of mass transfer is conducted by gradient in concentration of component(s). Fick's law of diffusion is also used for the calculation of molar flux of component *i*, N_i. It is written as a linear combination of the concentration gradients, $-dc_j/dz$, of all species [18]:

$$N_i = -\sum_{j=1}^{n} D_{ij} \frac{dc_j}{dz} \quad (1)$$

This formulation is phenomenological; the diffusion coefficients, D_{ij}, are obtained from experimental data and can be highly dependent on the concentrations.

The third approach for the calculation of multi-component mass transfer flux is irreversible thermodynamics. In this case, N_i is a linear combination of the chemical potential gradients, $-d\mu_j/dz$, which are the driving forces for diffusion:

$$N_i = -\sum_{j=1}^{n} L_{ij} \frac{d\mu_j}{dz} \quad (2)$$

The elements L_{ij} are called Onsager phenomenological coefficients which satisfy the relation $L_{ij}=L_{ji}$ between each pair of ions.

These three approaches can be further connected to other theories; see, for example, [19] for derivation of the MS equations from the classical Lagrange equations.

Among the different multi-component approaches, the MS equation has gained much attention. It has been used for modeling of some processes, such as diffusion in microporous membranes [20], pressure swing adsorption (PSA) [21], diffusion in carbon nanotubes [22], capillary diffusion [23], remediation of contaminated groundwater [24,25], membrane electrolysis process [26], gas transport in porous fuel cell anodes [27,28], enantiomer separation by chromatography [29] and membrane distillation [30]. Moreover, the MS equation is used to predict the diffusion, rather than in "standard" gas and liquid phases, such as in high-temperature gas nuclear reactors [31].

Membrane characterization and modeling of membrane processes are essential steps in the development and implementation of new membrane filtration processes. Several models, *e.g.* extended Nernst-Planck and Maxwell-Stefan, have been or are being developed for this purpose.

In NF process, generally steric hindrance (sieving effect), Donnan exclusion [32,33], dielectric exclusion [34] and/or increased solute solvation energy are counted responsible for the retention of solutes from solutions [35]. Mean pore radius, effective membrane thickness, and the surface charge density are the parameters required for Maxwell-Stefan model to predict the sieving and Donnan exclusion effects in the NF process [36,37]. These parameters are usually obtained by fitting the model parameters to solute retentions and membrane fluxes using pure water, single salt, and single sugar solutions. The number of model parameters will increase if dielectric exclusions (ε_p, ε_m) or changes in solvent structure are also taken into account.

We developed a comprehensive mathematical model for the prediction of ion transport through NF membranes. It is based on Maxwell-Stefan approach, which considers multi-component transport in two sections of the membrane system: feed boundary layer and membrane. Definitely, such a comprehensive model is unique in terms of establishing finite volume method of discretization for linearization and useful in designing new membrane systems for a wide variety of NF separations.

For simple geometries, one can show that all three methods of discretization (finite difference, finite element, and finite volume) produce the same solution matrix, whereas using the finite volume method enables the formulation for possible joining with CFD programs. On the other hand, the finite volume could be a better choice due to its unity weight function over discreted volume and exact global conservation, which is ensured for all grids, not only in the limit of grid refinement. The main advantages/novelties of this study, in comparison with similar works, could be summarized as:

1. Unlike the vast majority of the available literature which employs extended Nernst-Plank (ENP), this paper is based on generalized Maxwell-Stefan (GMS), which considers interactions of ion/ion, ion/solvent, solvent/membrane and ion/membrane.
2. The charge density is non-uniform along the pore, unlike many studies, considering probable ion adsorption to the pore wall through the Freundlich isotherm.
3. Dielectric exclusion is considered in partitioning when combined with GMS.
4. Good accuracy is obtained even for divalent cations.
5. Not assuming linear profile for electric potential and concentration through the membrane.
6. Using a simple relation for maintaining the concentration positive instead of using complex numerical method to minimize the positive penalty, which is the sum of residual of estimated and computational values of concentrations (negative concentration has no physical meaning).
7. The model and solving process have already been generalized for N components.
8. The provided procedure offers solving highly stiffed coupled equations of PDE, exponential, and algebraic, which powerful softwares are potentially incapable of solving, especially when the number of equations is increased as the number of components is increased.
9. Considering non-ideality of solution in terms of activity coefficient.

THEORY

1. Model Derivations

The main assumptions considered in this model are:

- All components have a constant molar flux at steady state conditions.

- The transport process in the membrane is isothermal. This assumption obviates the need for the solution of energy equation. Apparently, the assumption is allowed because no reaction, and therefore, no heat consumption or evolution takes place inside the membrane. Moreover, the heat generated due to ohmic resistance (calculated according to the method described by [18]) was estimated to be negligible.

For steady state conditions, the equation of continuity holds:

$$\frac{dN_i}{dz}=0 \quad i=1, 2, \ldots, n \tag{3}$$

Therefore, the molar fluxes are not functions of position in the membrane.

Two approaches are reviewed to calculate the molar fluxes of ions in the case of multi-component systems. The first one is Fick's law of diffusion:

$$J_i=-D_{i,s}\frac{dC_i}{dz} \tag{4}$$

C_i and J_i are molar concentration and flux of component *i*, respectively, $D_{i,s}$ is diffusion coefficient of component *i* in the solvent and z is the direction of diffusion. Fick's law of diffusion is valid if diffusion of a component occurs in the same direction as that of concentration gradient. However, Wesselingh and Krishna [17] demonstrated in an example the contravention of this phenomenon in which Na^+ ions in a solution of NaCl+HCl diffuse in the opposite direction of concentration gradient. Therefore, Fick's law of diffusion is not capable to describe such a phenomenon.

The second approach is derived from a force balance between frictional forces and driving ones. Krishna and Wesselingh [16] represented the above model in terms of:

$$\mathscr{F}_i=\sum_{k=1}^{N_c}\zeta_{i,k}x_k(u_i-u_k) \tag{5}$$

where denotes net $\mathscr{F}_i$ driving force acting on component *i* ($N\cdot mol^{-1}$). The term $\mathscr{F}_i$ consists of three potential gradients: chemical, pressure, and electric potential gradients. The right hand side (RHS) of Eq. (5) describes the total friction force between component *i* and other components by introducing $\zeta_{i,k}$ which is friction coefficient between components *i* and *k*. The effect of viscous flow, chemical potential, pressure, and thermodynamic non-idealities could be readily introduced in Eq. (5) considered as $\mathscr{F}_i$ (net driving force). Friction coefficient $\zeta_{i,k}$ is related to Maxwell-Stefan diffusion coefficient defined by Eq. (6) [17]:

$$\zeta_{i,k}=\frac{RT}{Đ_{i,k}} \tag{6}$$

As discussed earlier, net driving forces ($\mathscr{F}_i$) consist of three elements, including chemical potential gradient, pressure gradient, and electric potential gradient:

$$\mathscr{F}_i=\underbrace{-\nabla_T\mu_i}_{\substack{chemical\\ potential\\ gradient}}\ \underbrace{-V_i\nabla P}_{\substack{pressure\\ gradient}}\ \underbrace{-z_i\nabla\psi}_{\substack{electric\\ potential\\ gradient}} \tag{7}$$

where

$$\mu_i=\mu_i^o+RT\ln(\gamma_i c_i)+V_iP \tag{8}$$

Therefore, Eq. (5) is rearranged as:

$$-\nabla_{T,P}\mu_i-V_i\nabla P-z_iF\nabla\psi=\sum_k\zeta_{i,k}x_k(u_i-u_k) \tag{9}$$

By using Eq. (6) and multiplying Eq. (9) in x_i/RT, Eq. (10) is given as:

$$-\frac{x_i}{RT}\nabla_{T,P}\mu_i-\frac{x_i}{RT}V_i\nabla P-\frac{x_i}{RT}z_iF\nabla\psi=\sum_k\frac{x_ix_k(u_i-u_k)}{Đ_{i,k}} \tag{10}$$

Eq. (10) could become more complex by considering the membrane in an electrolyte solution. By introducing the membrane as a new component to the system, some additional parameters, such as diffusion coefficient in the membrane, porosity of membrane (ε), and tortuosity of the pores (τ), should be implemented in the equation. Since no information about mole fraction of the membrane (x_m) is available, it would be better to merge diffusion coefficient and mole fraction of the membrane in one term provided in Eq. (11):

$$\zeta_{i,m}=\frac{RT}{Đ_{i,m}} \tag{11}$$

Therefore, Eq. (10) is rearranged as Eq. (12) [37]:

$$-x_i\nabla_{T,P}\mu_i-x_iV_i\nabla P-x_iz_iF\nabla\psi=\sum_k\zeta_{i,k}\frac{\tau}{\varepsilon}x_ix_k(u_i-u_k)+\zeta_{i,m}\frac{\tau}{\varepsilon}x_iu_i \tag{12}$$

In pressure-driven membrane separation processes, such as nanofiltration, transport occurs not only due to diffusion, but also due to viscous forces [39]. As such, net velocity of each component (w_i) is equal to the summation of diffusion velocity (u_i) and viscous velocity (v_f):

$$w_i=u_i+v_f \tag{13}$$

Viscous velocity is also given by Eq. (14):

$$v_f=-\frac{\varepsilon B_0}{\tau\eta}\left(\Delta P+C_{tot}\sum_k x_kz_kF\nabla\psi\right) \tag{14}$$

where

$$B_0=\frac{r_p^2}{8} \tag{15}$$

Eq. (14) is simplified to the Hagen-Poiseuille equation for uncharged species, *i.e.*, pressure gradient of fluid with an average velocity of v_f through a pipe. The excess term in Eq. (14) is also the influence of membrane charge density on the transport of charged components and flow regime [39]. Substitution of Eqs. (13) and (14) in Eq. (12) gives:

$$-x_i\nabla_{T,P}\mu_i-x_i\left(V_i+\zeta_{i,m}\frac{\tau}{\varepsilon}\frac{\varepsilon B_0}{\tau\eta}\right)\nabla P-x_i\left(z_iF+\zeta_{i,m}\frac{\tau}{\varepsilon}\frac{\varepsilon B_0}{\tau\eta}C_{tot}\sum_k x_kz_kF\right)\nabla\psi$$
$$=\sum_k\zeta_{i,k}\frac{\tau}{\varepsilon}x_ix_k(w_i-w_k)+\zeta_{i,m}\frac{\tau}{\varepsilon}x_i(w_i) \tag{16}$$

By using the correlation which relates the molar flux of each com-

ponent (N_i) to velocity (w_i) and mole fraction of the component (x_i):

$$N_i = x_i w_i C_{tot} \tag{17}$$

Eq. (16) is rearranged as:

$$-x_i\nabla_{T,P}\mu_i - x_i\left(V_i + \zeta_{i,m}\frac{B_0}{\eta}\right)\nabla P - x_i\left(z_i + \zeta_{i,m}\frac{B_0}{\eta}C_{tot}\sum_k x_k z_k\right)F\nabla\psi = \frac{1}{C_{tot}}\left[\sum_k \zeta_{i,k}\frac{\tau}{\varepsilon}(x_k N_i - x_i N_k) + \zeta_{i,m}\frac{\tau}{\varepsilon}N_i\right] \tag{18}$$

By defining chemical potential ($\nabla_{T,P}\mu_i = RT\nabla(\ln\gamma_i x_i) = RT(\nabla(\gamma_i x_i)/\gamma_i x_i) \cong (RT/\gamma_i x_i)(dx_i/dy)$) and reducing the gradient operator to differential in a 1-dimentional system, Eq. (19) is obtained:

$$-\frac{RT}{\gamma_i}\frac{dx_i}{dy} - x_i\left(V_i + \zeta_{i,m}\frac{B_0}{\eta}\right)\frac{dP}{dy} - x_i\left(z_i + \zeta_{i,m}\frac{B_0 C_{tot}}{\eta}\sum_k x_k z_k\right)F\frac{d\psi}{dy} = \frac{1}{C_{tot}}\left[\sum_k \zeta_{i,k}\frac{\tau}{\varepsilon}(x_k N_i - x_i N_k) + \zeta_{i,m}\frac{\tau}{\varepsilon}N_i\right] \tag{19}$$

To apply the narrow pore size of membrane to the equations, hindrance factors are introduced in the GMS equation. This was developed by Noordman and Wesselingh [40] based on the work of Mason and Lonsdale [41] who also developed a modified form of the Maxwell-Stefan equation that accounts for the selective character of viscous flow. They inserted an empirical 'bugger factor', α_i', in the pressure term of the driving force. The final derivation is:

$$-\frac{RT}{\gamma_i}\frac{dx_i}{dy} - x_i\left(V_i + \zeta_{i,m}\alpha_i'\frac{B_0}{\eta}\right)\frac{dP}{dy} - x_i\left(z_i + \zeta_{i,m}\alpha_i'\frac{B_0 C_{tot}}{\eta}\sum_k x_k z_k\right)F\frac{d\psi}{dy} = \frac{1}{C_{tot}}\left[\sum_k \zeta_{i,k}\frac{\tau}{\varepsilon}(x_k N_i - x_i N_k) + \zeta_{i,m}\frac{\tau}{\varepsilon}N_i\right] \tag{20}$$

where

$$\alpha_i' = \frac{1}{\zeta_{i,m}}\left(\sum_k \zeta_{i,k}x_k(\alpha_i - \alpha_k)\right) + \alpha_i \tag{21}$$

In which

$$\alpha_i = (1 - 0.255\lambda_i - 1.279\lambda_i^{2.5} + 1.035\lambda_i^3)(2 - \varphi_i) \tag{22}$$

See Eqs. (28) and (32), respectively, for λ_i and φ_i. On the other hand, the diffusion coefficient of the Maxwell-Stefan equation for any combination of various species is not completely understood for arbitrary materials. Wesselingh et al. [42] developed sufficient data for predicting the order of magnitude of such diffusion coefficients. If a negatively charged membrane is utilized to reject ions from a solution, diffusion coefficients of water-matrix, anion-matrix, cation-water, and anion-water, are about 10^{-9} to 10^{-10} m^2/s, whereas the cation-matrix for a mono-valent cation is about 10^{-12} m^2/s. For di-/tri-valent cations this value might be reduced to 10^{-13} and 10^{-14} m^2/s, respectively.

For a system containing a single-electrolyte, diffusion coefficient of anion-cation is calculated through Eq. (23):

$$Đ_{+,-} = 2\left(\frac{1}{Đ_{+,w}} + \frac{1}{Đ_{-,w}}\right) \tag{23}$$

where the (+) sign refers to cations and (−) refers to anions. In the case of multi-electrolyte solutions, an experimental correlation is applied [37]:

$$Đ_{+,-} = \left(\frac{Đ_{+,w} + Đ_{-,w}}{2}\right)\frac{I_x^{0.55}}{|z_+ z_-|^{2.3}} \tag{24}$$

where $Đ_{+,w}$ and $Đ_{-,w}$ are diffusion coefficients of cations and anions in water, respectively, and I_x is the ionic strength, which is defined as:

$$I_x = \frac{1}{2}\sum z_i^2 x_i \tag{25}$$

The parameters $Đ_{+,+}$ and $Đ_{-,-}$ are estimated through distinctive equations. A number of diffusion coefficients compatible with the Maxwell-Stefan equation are listed in Table 1.

Table 1. Physical properties of ions compatible with Maxwell-Stefan model [42]

Component	$D_{i,w}\times10^{-9}$ (m^2/s)	$r_i\times10^{-9}$ (m)
Na^+	1.33	0.164
Cl^-	2.01	0.118
Ca^{2+}	0.78	0.276
H_2O	-	0.278

For other ions, $D_{i,w}$ is estimated through:

$$D_{i,w} = \frac{RT}{N_{avog}6\pi r_i\eta} \tag{26}$$

Friction factors of $\zeta_{i,m}$ and $Đ_{i,m}$ are estimated through an experimental correlation [43], which is derived from hard falling spheres in capillary tubes:

$$\zeta_{i,m} = \zeta_{i,w}\left(\frac{1}{(1-\lambda_i)^{2.2}} - 1\right) \tag{27}$$

where $\zeta_{i,m}$ and $\zeta_{i,w}$ are friction factors of component *i* with matrix and solvent (*e.g.* water), and λ_i is the ratio of stokes radius to pore radius of the ion:

$$\lambda_i = \frac{r_i}{r_p} \tag{28}$$

Now equations which are required for the prediction of ion transport through NF membrane are completed. Nevertheless, the formulations at both interfaces, *i.e.*, feed-membrane and membrane-permeate, are also required. Assuming thermodynamic equilibrium at both interfaces (Eqs. (29), (33)) and ignoring concentration polarization, *i.e.*, concentration at feed/membrane interface is equal to that of the bulk of the feed, $C_{i,0^-} = C_{i,b}$, it gives: (see Fig. 1)

$$\frac{\gamma_{i,0^+}c_{i,0^+}}{\gamma_{i,0^-}C_{i,0^-}} = \varphi_i \times \exp\left[-\frac{z_i F\Delta\psi_{D,0}}{RT}\right]\times\exp\left(-\frac{\Delta W_i}{k_B T}\right) \tag{29}$$

where

$$\Delta\psi_{D,0} = \psi_{0^+} - \psi_{0^-} \tag{30}$$

$$\Delta W_{i,Born} = \frac{(z_i e)^2}{8\pi\varepsilon_0 r_i}\left(\frac{1}{\varepsilon_p} - \frac{1}{\varepsilon_b}\right) \tag{31}$$

In which $\Delta W_{i,Born}$ is the Born salvation energy barrier, and

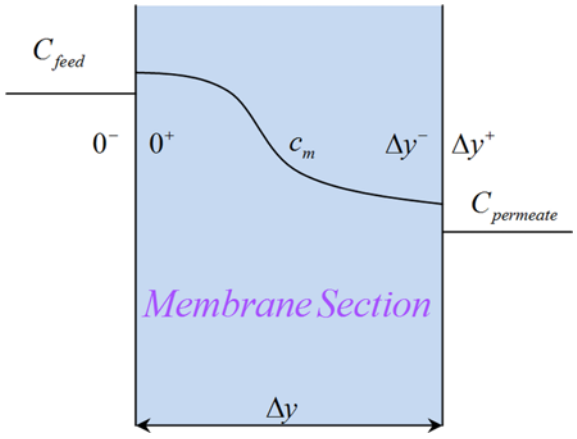

Fig. 1. Schematic of membrane cross section for ion transport.

$$\varphi_i=(1-\lambda_i)^2 \tag{32}$$

at the permeate side of the membrane [10]:

$$\frac{\gamma_{i,\Delta y^-}c_{i,\Delta y^-}}{\gamma_{i,\Delta y^+}C_{i,\Delta y^+}}=\varphi_i\times\exp\left[-\frac{z_iF\Delta\psi_{D,\Delta y}}{RT}\right]\times\exp\left(-\frac{\Delta W_i}{k_BT}\right) \tag{33}$$

Indeed, the thermodynamic equilibrium provided in Eqs. (29), (33) are corrected by three terms including steric restrictions (the first term of RHS), Donnan exclusion (the second term of RHS), and dielectric exclusion (the third term of RHS). Molar concentration of component *i* in Eq. (33) could be replaced by its mole fraction $x_i=c_i/C_{tot}$; $y_i=C_i/C_{tot}$. This equilibrium is common between Nernst-Planck and Maxwell-Stefan. However, in the case of Maxwell-Stefan model, another equilibrium is required in order to consider the solution: water. The latter is defined by Eq. (34):

$$RT\ln(\gamma_{0^-}^{solvent}y_{0^-}^{solvent})+V_iP_{0^-}=RT\ln(\gamma_{0^+}^{solvent}x_{0^-}^{solvent})+V_iP_{0^+} \tag{34}$$

where $y_{0^-}^{solvent}$ is mole fraction of solvent outside the membrane. Therefore;

$$\frac{\gamma_{0^-}^{solvent}y_{0^-}^{solvent}}{\gamma_{0^+}^{solvent}x_{0^+}^{solvent}}=\exp\left[\frac{V_i}{RT}(P_{0^+}-P_{0^-})\right] \tag{35}$$

Subscripts 0^- and 0^+ denote feed-side and membrane-side of the upper interface, respectively (see Fig. 1). Such a similar equation is also satisfied at the other interface of membrane-permeate:

$$\frac{\gamma_{\Delta y^+}^{solvent}y_{\Delta y^+}^{solvent}}{\gamma_{\Delta y^-}^{solvent}x_{\Delta y^-}^{solvent}}=\exp\left[\frac{V_i}{RT}(P_{\Delta y^-}-P_{\Delta y^+})\right] \tag{36}$$

Subscripts Δy^+ and Δy^- denote permeate-side and membrane-side of the lower interface, respectively (see Fig. 1).

Some other equations in the form of restrictions, including electroneutrality (Eq. (52)), charge balance inside membrane (Eq. (53)), component and total mass balance (Eq. (50)), and mole fraction summations (Eq. (51)), are also applied to make the number of variables equal to that of equations.

2. Solving the Model Equations

The governing equations are numerically solved to calculate the unknown variables including x_i, ψ, pressure inside the membrane, $x_{i,permeate}$, $\psi_{permeate}$, and molar flux of each component. The model equations consist of ordinary differential, partial differential, exponential, non-linear, and algebraic equations. Simultaneous solution of this set of equations is possible by linearization of the system in order to deal with linear equations instead of a complex set of equations. Linearization is carried out in this work by applying Taylor expansion for the following multi-variable function:

$$f(u,v)\cong f(u^*,v^*)+\left.\frac{\partial f}{\partial u}\right|_{u^*,v^*}\times(u-u^*)+\left.\frac{\partial f}{\partial v}\right|_{u^*,v^*}\times(v-v^*) \tag{37}$$

Superscript (*) represents the value of the assigned variable in the previous iteration of the solving loop. In each iteration, all linearized equations are solved using a matrix of AX=B to find X. Here A is square matrix of coefficients, B is vector of constants, and X is the unknown vector. New values of unknown variables would then update the matrix A and vector B.

The equations which need linearization include partitioning equa-

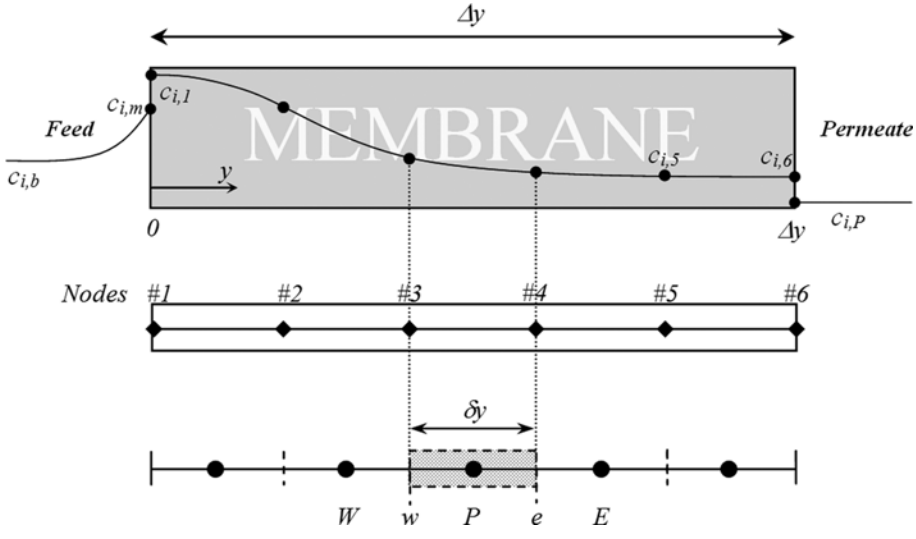

Fig. 2. Schematic representation of membrane compartment and discretization.

Table 2. Mole fraction's coefficient in j^{th} grid node for i^{th} component in discretized GMS, Eq. (39)

Mole fraction	Coefficient
$x_{1,j}$	$A_{1,j}=\frac{\zeta_{i,1}N_i^*}{2C_{tot}}$
$x_{2,j}$	$A_{2,j}=\frac{\zeta_{i,2}N_i^*}{2C_{tot}}$
⋮	⋮
$x_{i,j}$	$A_{i,j}=\frac{\zeta_{i,i}N_i^*}{2C_{tot}}+\frac{RT}{\delta y}-\frac{\theta_i}{2\delta y}(P_{j+1}^*-P_j^*)-\frac{\beta_i}{2\delta y}(\psi_{j+1}^*-\psi_j^*)+\sum_k\zeta_{i,k}(x_{k,j}^*+x_{k,j+1}^*)$
⋮	⋮
$x_{NC,j}$	$A_{NC,j}=\frac{\zeta_{i,NC}N_i^*}{2C_{tot}}$

Table 3. Mole fraction's coefficient in $j+1^{th}$ grid node for i^{th} component in discretized GMS, Eq. (39)

Mole fraction	Coefficient
$x_{1,j+1}$	$B_{1,j}=\frac{\zeta_{i,1}N_i^*}{2C_{tot}}$
$x_{2,j+1}$	$B_{2,j}=\frac{\zeta_{i,2}N_i^*}{2C_{tot}}$
⋮	⋮
$x_{i,j+1}$	$B_{i,j}=\frac{\zeta_{i,i}N_i^*}{2C_{tot}}-\frac{RT}{\delta y}-\frac{\theta_i}{2\delta y}(P_{j+1}^*-P_j^*)-\frac{\beta_i}{2\delta y}(\psi_{j+1}^*-\psi_j^*)+\sum_k\zeta_{i,k}(x_{k,j}^*+x_{k,j+1}^*)$
⋮	⋮
$x_{NC,j+1}$	$B_{NC,j}=\frac{\zeta_{i,NC}N_i^*}{2C_{tot}}$

tion at feed/membrane interface, partitioning equation at membrane/permeate interface, and Maxwell-Stefan equation. Since the Maxwell-Stefan equation should be solved along the membrane pore, therefore discretization needs to be performed along the pore. Discretization has been conducted using finite volume method. The membrane pore is divided into M internal grids (for inside the pore) and two grids at both interfaces. A schematic representation of membrane compartment and discretization procedure is provided in Fig. 2.

A number of M grids inside the membrane would generate M−1 control volumes. Maxwell-Stefan is applied as a mass transport model to each control volume. Employing finite volume method to Eq. (19), GMS would result in linearized form of Eq. (38). The details on the procedure for obtaining Eq. (38) are provided in Part A of supplementary materials.

$$
\begin{aligned}
&-\frac{RT}{\gamma_i}((x_i)_e-(x_i)_w)\\
&-\beta_i\left(\frac{(x_i^*)_w+(x_i^*)_e}{2}((\psi)_e-(\psi)_w)+\nabla\psi^*\left(\frac{(x_i)_w+(x_i)_e}{2}-\frac{(x_i^*)_w+(x_i^*)_e}{2}\right)\delta y\right)\\
&-\theta_i\left(\frac{(x_i^*)_w+(x_i^*)_e}{2}((P)_e-(P)_w)+\nabla P^*\left(\frac{(x_i)_w+(x_i)_e}{2}-\frac{(x_i^*)_w+(x_i^*)_e}{2}\right)\delta y\right)\\
&=\frac{\tau}{\varepsilon}\frac{1}{C_{tot}}\left[\sum_k\zeta_{i,k}\left[\begin{array}{l}\frac{(x_k^*)_w+(x_k^*)_e}{2}N_i+N_i^*\left(\frac{(x_k)_w+(x_k)_e}{2}-\frac{(x_k^*)_w+(x_k^*)_e}{2}\right)\cdots\\ -\frac{(x_i^*)_w+(x_i^*)_e}{2}N_k-N_k^*\left(\frac{(x_i)_w+(x_i)_e}{2}-\frac{(x_i^*)_w+(x_i^*)_e}{2}\right)\end{array}\right]\right.\\
&\left.+\zeta_{i,m}N_i\right]\times\delta y
\end{aligned}
\tag{38}
$$

By replacing "e" and "w" subscripts with the grid node counters, *j+1* and *j*, the unknown variables would be rewritten in the form of $x_{i,j}$ or $x_{i,j+1}$, N_i or N_{i+1}, P_j or P_{j+1}, and ψ_j or ψ_{j+1}.

It is important to determine the coefficient of each variable in each equation. Eq. (38) thus needs to be expanded in order to detect the coefficients. In this way, all the mole fraction coefficients provided in Tables 2 and 3 as well as molar flux coefficients provided in Table 4 will be obtained. Note that due to the summation in the first term of right hand side of Eq. (38), all of mole fractions and molar fluxes are involved in each GMS equation through each control volume.

Table 4. Molar flux's coefficient in discretized GMS

Molar flux	Coefficient
N_1	$C_{1,j}=\frac{\zeta_{i,1}N_i^*}{2C_{tot}}$
N_2	$C_{2,j}=\frac{\zeta_{i,2}N_i^*}{2C_{tot}}$
⋮	⋮
N_i	$C_{i,j}=\frac{\zeta_{i,i}N_i^*}{2C_{tot}}-\frac{1}{2C_{tot}}\sum\zeta_{i,k}(x_{k,j}^*+x_{k,j+1}^*)-\frac{\zeta_{i,m}}{C_{tot}}$
⋮	⋮
N_{NC}	$C_{NC,j}=\frac{\zeta_{i,NC}N_i^*}{2C_{tot}}$

$$\sum_k A_{k,j}x_{k,j}+\sum_k B_{k,j}x_{k,j+1}+\sum_k C_{k,j}N_k+D_{i,j}P_j + E_{i,j}P_{j+1}+F_{i,j}\psi_j+G_{i,j}\psi_{j+1}=H_{i,j} \quad (39)$$

Also, the pressure coefficients in j^{th} and $j+1^{th}$ grid nodes and those for electric potential do not need to be provided in a table because the coefficients are the same for all components:

$$D_{i,j}=\frac{\theta_i}{2\delta y}(x^*_{i,j}+x^*_{i,j+1}) \quad (40)$$

$$E_{i,j}=-\frac{\theta_i}{2\delta y}(x^*_{i,j}+x^*_{i,j+1}) \quad (41)$$

$$F_{i,j}=\frac{\beta_i}{2\delta y}(x^*_{i,j}+x^*_{i,j+1}) \quad (42)$$

$$G_{i,j}=\frac{\beta_i}{2\delta y}(x^*_{i,j}+x^*_{i,j+1}) \quad (43)$$

$$H_{i,j}=\frac{1}{2C_{tot}}\sum\zeta_{i,k}(N^*_k(x^*_{i,j}+x^*_{i,j+1})-N^*_i(x^*_{k,j}+x^*_{k,j+1}))\ldots - \frac{\theta_i}{2\delta y}(x^*_{i,j}+x^*_{i,j+1})(P^*_{j+1}-P^*_j)-\frac{\beta_i}{2\delta y}(x^*_{i,j}+x^*_{i,j+1})(\psi^*_{j+1}-\psi^*_j) \quad (44)$$

The linear form of GMS is applied to each control volume (between each two grids). Investigation of the number of equations and unknown variables as well as degrees of freedom is given in Tables 5 and 6.

3. Linearized form of Partitioning Equations at Interfaces

Eqs. (35) and (36) are in the form of exponential equations. Going through the linear system, they need to be also linearized using Eq. (37). Linear form of Eq. (35) is:

$$\left\langle \gamma^{solvent}_{0^+}\right\rangle x^{solvent}_{0^+}+\left\langle \gamma^{*,solvent}_{0^-}y^{*,solvent}_{0^-}\frac{V_i}{RT}\exp\left[\frac{V_i}{RT}(P^*_{0^-}-P^*_{0^+})\right]\right\rangle P_{0^+} - \left\langle \gamma^{solvent}_{0^-}\exp\left[-\frac{V_i}{RT}(P^*_{0^+}-P^*_{0^-})\right]\right\rangle y^{solvent}_{0^-} = -\left\langle \gamma^{*,solvent}_{0^-}y^{*,solvent}_{0^-}\exp\left[-\frac{V_i}{RT}(P^*_{0^+}-P^*_{0^-})\right]\frac{V_i}{RT}(-P^*_{0^+})\right\rangle \quad (45)$$

and linear form of Eq. (36) is:

$$\left\langle \gamma^{solvent}_{\Delta y^-}\right\rangle x^{solvent}_{\Delta y^-}-\left\langle \gamma^{solvent}_{\Delta y^+}\exp\left[-\frac{V_i}{RT}(P^*_{\Delta y^-}-P^*_{\Delta y^+})\right]\right\rangle y^{solvent}_{\Delta y^+} + \left\langle \gamma^{*,solvent}_{\Delta y^+}y^{*,solvent}_{\Delta y^+}\frac{V_i}{RT}\exp\left[\frac{V_i}{RT}(P^*_{\Delta y^+}-P^*_{\Delta y^-})\right]\right\rangle P_{\Delta y^-}= - \left\langle \gamma^{*,solvent}_{\Delta y^+}y^{*,solvent}_{\Delta y^+}\exp\left[-\frac{V_i}{RT}(P^*_{\Delta y^-}-P^*_{\Delta y^+})\right]\frac{V_i}{RT}(P^*_{\Delta y^+}-P^*_{\Delta y^-}) - \gamma^{*,solvent}_{\Delta y^+}y^{*,solvent}_{\Delta y^+}\frac{V_i}{RT}\exp\left[\frac{V_i}{RT}(P^*_{\Delta y^+}-P^*_{\Delta y^-})\right]P_{\Delta y^+}\right\rangle \quad (46)$$

Also linear form of Eq. (29) would be

$$\langle\gamma^*_{i,0^+}\rangle x_{i,0^+}-\left\langle \gamma^*_{i,0^-}\varphi_i\exp\left(-\frac{\Delta W_i}{k_BT}\right)\exp\left[\frac{z_iF}{RT}(\psi^*_{0^-}-\psi^*_{0^+})\right]\right\rangle y_{i,0^-} + \left\langle y^*_{i,0^-}\gamma^*_{i,0^-}\varphi_i\exp\left(-\frac{\Delta W_i}{k_BT}\right)\left(\frac{z_iF}{RT}\right)\exp\left[\frac{z_iF}{RT}(\psi^*_{0^-}-\psi^*_{0^+})\right]\right\rangle\psi_{0^+} - \left\langle y^*_{i,0^-}\gamma^*_{i,0^-}\varphi_i\exp\left(-\frac{\Delta W_i}{k_BT}\right)\left(\frac{z_iF}{RT}\right)\exp\left[\frac{z_iF}{RT}(\psi^*_{0^-}-\psi^*_{0^+})\right]\right\rangle\psi_{0^-} = \left\langle y^*_{i,0^-}\gamma^*_{i,0^-}\varphi_i\exp\left(-\frac{\Delta W_i}{k_BT}\right)\left(\frac{z_iF}{RT}\right)\exp\left[\frac{z_iF}{RT}(\psi^*_{0^-}-\psi^*_{0^+})\right](\psi^*_{0^+}-\psi^*_{0^-})\right\rangle \quad (47)$$

Same procedure has been applied to Eq. (33):

$$\langle\gamma^*_{i,\Delta y^-}\rangle x_{i,\Delta y^-}-\left\langle \gamma^*_{i,\Delta y^+}\varphi_i\exp\left(-\frac{\Delta W_i}{k_BT}\right)\exp\left[\frac{z_iF}{RT}(\psi^*_{\Delta y^+}-\psi^*_{\Delta y^-})\right]\right\rangle y_{i,\Delta y^+} + \left\langle y^*_{i,\Delta y^+}\gamma^*_{i,\Delta y^+}\varphi_i\exp\left(-\frac{\Delta W_i}{k_BT}\right)\left(\frac{z_iF}{RT}\right)\exp\left[\frac{z_iF}{RT}(\psi^*_{\Delta y^+}-\psi^*_{\Delta y^-})\right]\right\rangle\psi_{\Delta y^-} - \left\langle y^*_{i,\Delta y^+}\gamma^*_{i,\Delta y^+}\varphi_i\exp\left(-\frac{\Delta W_i}{k_BT}\right)\left(\frac{z_iF}{RT}\right)\exp\left[\frac{z_iF}{RT}(\psi^*_{\Delta y^+}-\psi^*_{\Delta y^-})\right]\right\rangle\psi_{\Delta y^+} = \left\langle y^*_{i,\Delta y^+}\gamma^*_{i,\Delta y^+}\varphi_i\exp\left(-\frac{\Delta W_i}{k_BT}\right)\left(\frac{z_iF}{RT}\right)\exp\left[\frac{z_iF}{RT}(\psi^*_{\Delta y^+}-\psi^*_{\Delta y^-})\right](\psi^*_{\Delta y^-}-\psi^*_{\Delta y^+})\right\rangle \quad (48)$$

Table 5. Degree of freedom - population of equations

Equation	Population	Details
GMS, Eq. (38)	$N_c(M-1)$	*For each component in each control volume*
Partitioning, Eq. (45)-(48)	N_c+N_c	*For each component at both interfaces*
Electroneutrality, Eq. (52)	1	*At permeate interface grid*
Charge balance, Eq. (55)	M	*For all components at each grid inside membrane*
Mass balance, Eq. (50)	N_c-1	N_c-1 *"non-repetitive" equations*
Mole fraction summation, Eq. (51)	M+1	*At each grid inside +1 at permeate interface grid*
Total	$N_c+(M+1)(2+N_c)-1$	

Table 6. Degree of freedom - population of variables

Variables	Population	Details
Mole fraction (x_i)	$N_c\times(M+1)$	*M grids inside +1 at permeate interface grid for N_c components*
Electric potential (ψ)	M+1	*M grids inside +1 at permeate interface grid*
Pressure (P)	M	*M grids inside*
Flux of components (N_i)	N_c	-
Total	$N_c+(M+1)(2+N_c)-1$	

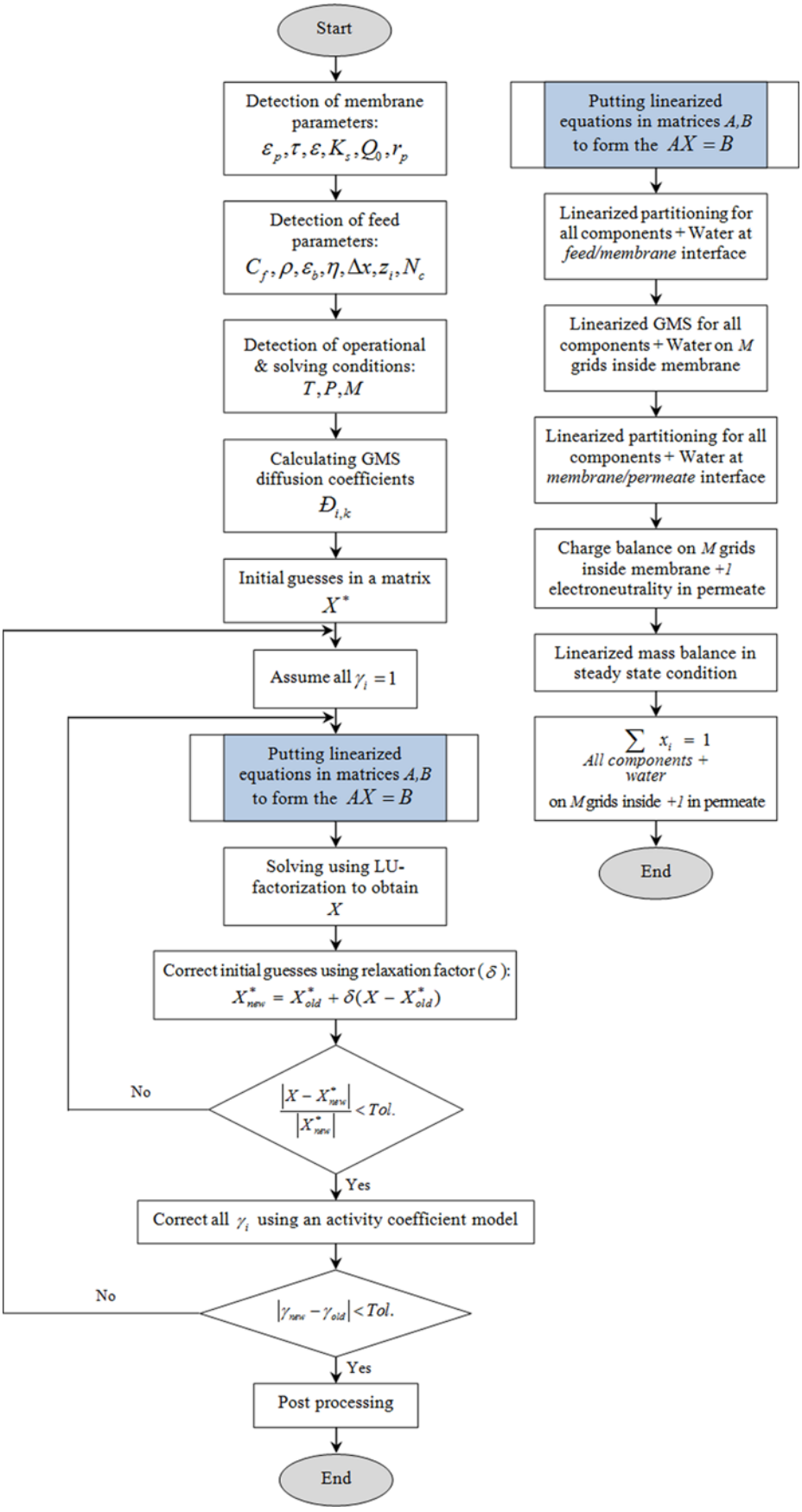

Fig. 3. Solving procedure and sub-procedure's flow chart.

4. Governing Conditions and Restrictions

Four governing conditions, including the mass balance on permeate, summation of mole fractions, electroneutrality in the permeate side, and charge balance within the membrane, are present in the system which should be implemented into the model equations. By implementing the latter conditions the degree of freedom will become zero.

- Mass balance on permeate

The main relation for the mass balance on the permeate side is introduced by Eq. (49):

$$\frac{N_i}{N_w}=\frac{y_{i,p}}{y_{w,p}} \tag{49}$$

After linearization, Eq. (49) will become in the form of Eq. (50):

$$\langle y^*_{w,p}\rangle N_i+\langle N^*_i\rangle y_{w,p}-\langle y^*_{i,p}\rangle N_w-\langle N^*_w\rangle y_{i,p}=\langle N^*_i y^*_{w,p}-N^*_w y^*_{i,p}\rangle \tag{50}$$

- Mole fraction summation:

$$\begin{aligned}&\sum x_i=1\\&\sum y_i=1\end{aligned} \tag{51}$$

No linearization is needed.

- Electroneutrality in the permeate side:

$$\sum\langle z_i\rangle y_i=0 \tag{52}$$

which is already linear.

- Charge balance inside the membrane:

$$\sum\langle z_i\rangle x_i+\frac{X}{C_{tot}}=0 \tag{53}$$

where X is the net charge per unit volume (charge density) in which X is related to the mole fraction by following isotherms (deduced from [37]):

$$\frac{X}{C_{tot}}=-Q^*\left(\sum|z_i|x_i\right)^{K_s} \tag{54}$$

The details of linearization are presented in Part B of supplementary materials, while the final result would be:

$$\sum_i\left\langle z_i-Q^*|z_i|K_S\left(\sum_k|z_k|x^*_k\right)^{K_s-1}\right\rangle x_i=Q^*\left(\sum_k|z_k|x^*_k\right)^{K_s}(1-K_S) \tag{55}$$

With regards to the second claim alluded in section 1 (introduction), the model is capable of considering membrane charge density within the governing equation, more closer to actual conditions (adsorption of ions to the pore wall and consequent non-uniform charge density), while it does not jeopardize the agreement between experimental results and predictions.

5. Degree of Freedom (DOF)

Assuming $\psi_0=0$ as the reference and $P_{\Delta y^*}=0$ as atmospheric outlet, the equations and variables for a system consisting of N_c components (solvent+electrolyte), which is discretized to M grids inside the membrane added by two grids at both interfaces, are provided in Tables 5 and 6, respectively.

According to data provided in Tables 5 and 6, the degree of freedom is equal to zero due to equality of variables and equations. Therefore, the set of equations would have a singular solution. The flowchart introduced in Fig. 3 represents the solving procedure. Meanwhile, the vector of unknown variables and complementary explanations are provided in Appendix A.

6. Iterative Process of Solving

Matrix of coefficient that is captured through linearized equations could be solved via values of initial guess as the first iteration. At the next step, the matrix of coefficients and vector of constants must be updated by substituting values of such coefficients with that of calculated in previous iteration. The same goes for the subsequent iterations. Oftentimes, continuing this iterative method to deal with the non-linear set of equations indicates numerical instability (*i.e.*, divergence or oscillation) during the solving process. To achieve converged iterations [44] suggested a relaxation method that ensures more reliable convergence with bounded values.

Two different, but similar, relations of relaxation were employed for mole fraction and pressure/electric potential. The reason would be that the former is always positive while both the latter can take positive or negative values. The pressure and electric potential are assumed to be zero on the last node (as reference value). The following relaxation formulas are used:

$$\begin{aligned}&\psi^{new}=\psi^{old}+\delta(\psi^{calculated}-\psi^{old})\\&P^{new}=P^{old}+\delta(P^{calculated}-P^{old})\end{aligned} \tag{56}$$

where δ is the relaxation factor, which usually is between $0<\delta\leq 1$ known as under-relaxation factor. With this formula, the relaxed value ψ^{new} drops between the value of the previous iteration ψ^{old} and the value calculated through solving the linearized system of equations, *i.e.* $\psi^{calculated}$. If one employs no relaxation factor, so $\delta=1$ and then $\psi^{new}=\psi^{calculated}$, as expected.

Slightly different relaxation scheme was used for the mole fractions of the species. Here, one must ensure that the mole fractions are always positive and maintained (negative mole fractions are physically unreliable). The following relaxation scheme ensures this condition:

$$x_i^{new}=x_i^{old}+\delta(x_i^{calculated}-x_i^{old})\min\left(\left|\frac{x_i^{old}}{x_i^{calculated}-x_i^{old}}\right|,1\right) \tag{57}$$

The last term that is multiplied, ensures that even when $((x_i^{calculated}-x_i^{old})/x_i^{old})\geq 1$, the maximum value of $\min(|x_i^{old}/(x_i^{calculated}-x_i^{old})|, 1)$ is ≤ 1. So, with accordance to Eq. (57), the value of x_i^{new} is not going to become negative.

The activity coefficients which are used in GMS as well as membrane interface equilibriums (called partitioning) are also converging in an inner loop for a single iteration (because they are depending on the calculated concentration by their own). Of course it increases the time of convergence, but almost all studies in this regard ignore the non-ideality of electrolytes and assume the activity coefficients equal unity (refer to claim #9).

RESULTS AND DISCUSSION

The experimental results which are introduced in this paper from Déon et al. [8] are those which have been extrapolated at infinite feed flow rate. At this condition concentration polarization could be called off while it has no impact on the results as shown by Déon

Table 7. Properties of solutions based on [8]

Ion	Concentration of ions in solution (mol/m^3)					
	$NaCl/Na_2SO_4$			$NaCl/MgCl_2$		
	90/10	50/50	10/90	90/10	50/50	10/90
Na^+	50	50	50	45	25	5
Cl^-	45	25	5	50	50	50
3rd Species†	2.5	12.5	22.5	2.5	12.5	22.5

†3rd Species in $NaCl/Na_2SO_4$ system is SO_4^{2-} while that in $NaCl/MgCl_2$ one is Mg^{2+}

et al. [45]. The supplied membrane was a polyamide film one which was operating under cross-flow conditions.

The mesh network is decided (after optimizing computing time and mesh independency) to include 30 nodes at the active layer. Properties of considered solutions are introduced in Table 1, while concentrations of systems introduced in sections 3.1 and 3.2 are given in left and right-hand side of Table 7, respectively. Other properties of the system are found in Table 8.

It should be mentioned that numerical testing in Geraldes and Brites Alves (2008) shows that the major cause for the stiff behavior of such systems would be the difference of scales between the diffusion coefficients (*e.g.*, $D_{Na^+}=0.302\times10^{-9}$ m^2/s and $D_{Mg^{2+}}=0.429\times10^{-11}$ m^2/s) inside the membrane (refer to steric hindrance, Eq. (22)). So, a similar stiff system introduced in Geraldes and Brites Alves [12] is fed to our model and results are compared in supplementary materials part C. The comparison shows our model is also capable of dealing with stiffness well (Proof of claim #8).

1. Electrolyte Systems of NaCl and Na_2SO_4

In this section, simulation results and tuning for electrolyte system of are discussed. The results are compared with the experimental data reported by Déon et al. [8]. Three mixtures with molar ratios of 90/10, 50/50, and 10/90 of $NaCl/Na_2SO_4$ were considered in the simulations. These proportions correspond to the ratio of the charge concentrations (*i.e.*, in eq/m^3) of non-common ions, the ratio corresponding to the monovalent and divalent percentages. The rejections for these ions are reported in the experimental work

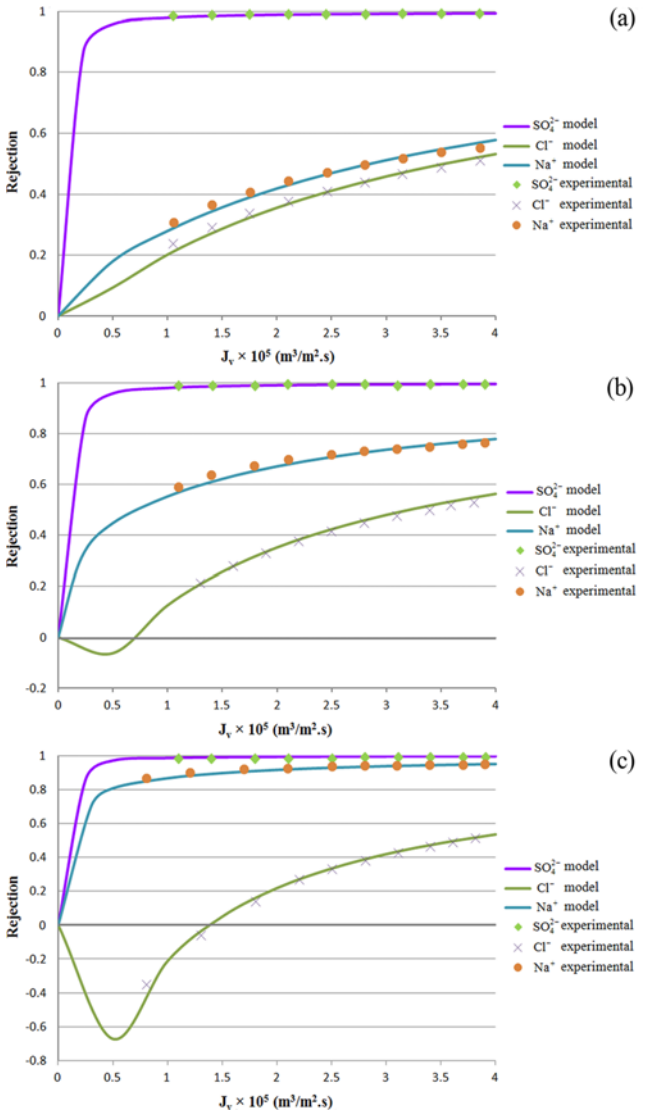

Fig. 4. Comparison of simulated and experimental rejection curves for solutions containing various molar ratios of $NaCl/Na_2SO_4$ (a) 90/10 (b) 50/50 (c) 10/90.

Table 8. GMS model parameters considering in NF system

Parameters	Description	Value	Reference
T	Temperature (K)	298	Room temperature
$r_{i,s}$	Stokes radii of ions (10^{-10} m) $Na^+/Cl^-/SO_4^{2-}/Mg^{2+}$	1.84/1.21/2.31/3.48	[6]
r_p	Mean pore radius (10^{-9} m)	0.53	[8]
ε_b	Water dielectric constant at 25 °C	78.4	[7]
L_p	Membrane permeability (10^{-14} m^{3}m^{-2})	1.6	[8]
η	Water dynamic viscosity (Pa·s)	0.9	Global
ε_p	Pore dielectric constant	To be fitted	-
Q^*	Freundlich parameters	To be fitted	-
K_s	Freundlich parameter	To be fitted	-
C_i	Species molar fraction at feed side	Given for each mixture	-
J_v	Water flux	Varies to calculate rejection	-
γ_i	Activity coefficient of species	Converging in an inner loop	-

Table 9. Fitted parameters of K_s, Q^* and ε_p

	Systems					
	$NaCl/Na_2SO_4$			$NaCl/MgCl_2$		
	90/10	50/50	10/90	90/10	50/50	10/90
% 3rd Species†	5	33	82	5	33	82
K_s	0.008	0.009	0.006	0.057	0.054	0.056
Q^*	-8.984×10^{-5}	-1.157×10^{-5}	-0.203×10^{-5}	-4.851×10^{-4}	-1.799×10^{-4}	-0.929×10^{-4}
ε_p	45.401	39.924	33.809	54.04	51.19	47.88
Accuracy	1.0×10^{-5}	1.3×10^{-4}	9.5×10^{-5}	2.4×10^{-3}	2.2×10^{-3}	1.3×10^{-3}

†3rd Species in $NaCl/Na_2SO_4$ system is SO_4^{2-} while that in $NaCl/MgCl_2$ one is Mg^{2+}

of Déon et al. [8]. Note that the concentration polarization layer is not considered in this simulation due to the dilution of solutions. The concentrations of ions in the solutions are listed in Table 7.

Mesh independency test was performed in the active layer of membrane and it was clear that the optimum number of meshes is M=50. Other parameters of the considered system are briefly reported in Table 8.

Comparisons between observed and calculated rejections are shown in Fig. 4(a), (b), (c). Q^*, K_s and ε_p are chosen as model parameters with respect to Eq. (58). The values of these fitted parameters are also given in the left-hand side of Table 9. To fit the parameters, Eq. (58) should be minimized:

$$Q=\frac{1}{n\times m}\sum_{1}^{m}\sum_{1}^{n}(R_{exp}-R_{sim}) \tag{58}$$

where n and m are the number of experiments and ions, respectively. Parameters R_{exp} and R_{sim} refer to experimental and predicted rejections, respectively. To be the foremost comprehensive model introduced so far, and determining the governing equations, the dielectric exclusion effect (third term in Eq. (29)) is also considered; meanwhile some studies such as Afonso and de Pinho [46], Bowen et al. [47], Schaep et al. [48] did not. Since ε_p is a key parameter for the solvent that measures the capability of carrying ions and the ability of storing electrical energy, therefore it seems necessary to be involved in the model. Due to limitation of figures we prefer not to demonstrate the results gathered without adjustable parameter ε_p which serves as importance of dielectric effect of the model (with accordance to claim #3). A further discussion would be presented on this topic, but as we are more interested in the ions competition and contribution in rejection, this was offered earlier (in this and next section).

It is indicated that rejection of SO_4^{2-} is frequently near unity in all three solutions. The reason for this behavior is high electric charges density of membrane opposed against entrance of this ion into the membrane pores (in fact the membrane charge is negative), although the ion diameter is smaller than membrane pores, and charge exclusion prevails. This observation confirms that the Donnan effect is predominant in comparison with steric hindrance. Another reason is that the Born Eq. (31) is proportional to square of the ion charges [9]. Therefore, the hindrance shows a resistance four times greater than those for monovalent ions against dissolution of SO_4^{2-} (see Eqs. (33)-(36)). By increasing the amount of SO_4^{2-} in the solutions, Figs. 4 ((a) towards (c)), rejection of Na^+ increases while rejection of Cl^- decreases. The latter observation is attributed to high rejection of SO_4^{2-} which enforces Na^+ ions to remain in the feed side to insure the electroneutrality conditions. This tendency is opposite for Cl^- ions, so Cl^- ions are transferred to the permeate side. Furthermore, by comparing diffusivities, it is obvious that Cl^- diffusivity is higher than those for other ions while its radius is the smallest. This phenomenon increases the probability of permeation for Cl^- through the membrane. In other words, the latter phenomenon explains the observation of negative rejection at the condition where SO_4^{2-} concentration is high and Cl^- concentration is low. It means that Cl^- ions are pushed to the permeate side in the presence of SO_4^{2-} ions and, therefore, rejection decreases in comparison with the condition at which no SO_4^{2-} ion presents, *i.e.*, pure NaCl, and may even reach negative values.

For higher fluxes of permeate, as expected, rejection of all species increased, due to higher pass of water molecules. On the other hand, to satisfy electroneutrality condition in permeate side, one Na^+ ion must be transported with each Cl^- ion. Since concentration of Na^+ ions in the feed is higher than that of Cl^- ions, therefore the observed rejection of Na^+ is higher than that for Cl^-. This event intensifies by decreasing Cl^- concentration in the feed side (Fig. 4(c)).

Profiles of concentrations and electric potentials of three ions for all expected conditions at constant $J_v(=2\times10^{-5}\ m^3/m^2\cdot s)$ are shown in Fig. 5(a), (b), (c). In all figures, the concentration of SO_4^{2-} inside the membrane is about zero, as a result of high rejection by the membrane. Also Cl^- and Na^+ concentrations are equal in the permeate side to satisfy electroneutrality condition. By decreasing the amount of Cl^- ions and increasing SO_4^{2-} ions in the feed solution (from Fig. 5(a) toward Fig. 5(c)) and with respect to approximately equal portion of Na^+ ions in three cases, rejection of Na^+ increases with SO_4^{2-} ions in the feed; therefore, fewer Na^+ enter the membrane pores (Fig. 4(c) compared with Fig. 4(a)) and because of more rejection of Na^+, the concentration of this ion and also Cl^- in the permeate side decreases.

2. Electrolyte Systems of NaCl and $MgCl_2$

In this section, the predictions and tuning of the developed model for an electrolyte system consisting of NaCl & $MgCl_2$ are introduced. The investigation includes three mixtures of different molar ratios of $NaCl/MgCl_2$ proportional to 90/10, 50/50 and 10/90 based on Déon et al. [8], while the model predicts the rejection of constituent ions.

Fig. 6(a), (b), (c) demonstrate results of experiments (taken from Déon et al. [8] and predictions of the current simulation. Parame-

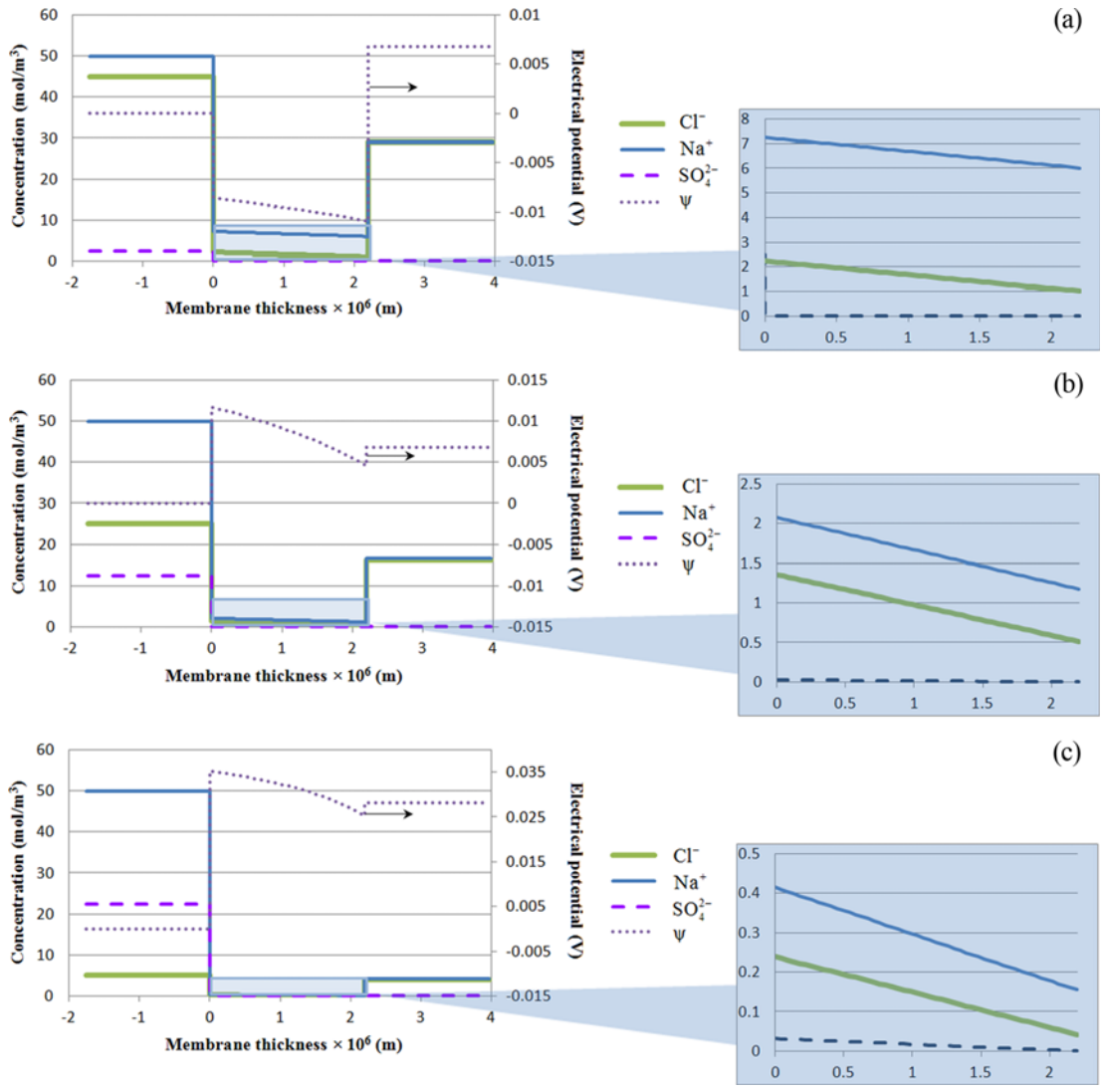

Fig. 5. Concentration and electric potential profile (a) 90/10 (b) 50/50 (c) 10/90.

ters Q^*, K_s and ε_p are used as adjustable parameters to tune the responses. The values of these fitted parameters are also given in right-hand side of Table 9. The aforementioned parameters have been chosen where Eq. (58) is minimized again.

As it is shown in Fig. 6 that rejection of Mg^{2+} cation is increased from Fig. 6(a) to 6(c), while rejection of Na^+ cation is decreased at the time concentration of Cl^- anion is approximately constant regarding the data provided in Table 9. Actually, various concentrations of Mg^{2+} have been employed within the suggested mixtures.

Fig. 6(a) could be discussed in such a way that at low concentration of Mg^{2+} cation, almost equal rejection of Na^+ and Cl^- ions would observed (due to Eq. (53)).

In the case of solutions with no $MgCl_2$, similar condition would be obtained. The tiny difference between former and earlier case is due to the presence of Mg^{2+} cations. Description of Fig. 6(c) (concentrated solution of $MgCl_2$) is closely related to that of Fig. 6(a), and almost equal rejection of Mg^{2+} and Cl^- ions is attained due to simultaneous movement of ions. It is clear that rejection of Cl^- from Figs. 6(a) to 6(c) is getting apart from that of Na^+ and joins to Mg^{2+} retention. In fact, as Mg^{2+} increases and Na^+ decreases; Na^+ cations are rejected to the permeate side in order to satisfy electroneutrality. On the other hand, Na^+ ions are accompanied with Cl^- ions passing through the membrane. Since Cl^- anions concentration is high in the feed side while concentration of Na^+ cations is low, the negative rejection values would be observed (facilitated transportation of ions). In this case, rejection of Cl^- ions is positive yet, and this effect will be intensified at lower concentrations of Na^+ and higher concentrations of Mg^{2+}.

Finally, for the reasons of greater diffusion coefficient ratio of Na^+ to Mg^{2+} (≈2 times), less positive charge (weaker dielectric effect), and less stocks ion radius ratio of Na^+ compared to Mg^{2+} (≈0.5 time), the transport of this ion (from feed side to permeate side) would potentially be increased in a manner that gives rise to higher permeate concentration of Na^+ in comparison with feed concentration (negative rejection). The reason for increment within the rejection from Fig. 6(a) to 6(b) is decreasing the absolute value of membrane charge density (which is directly related to Q^* according to Eq. (54)); besides, the dielectric constant of the solution inside

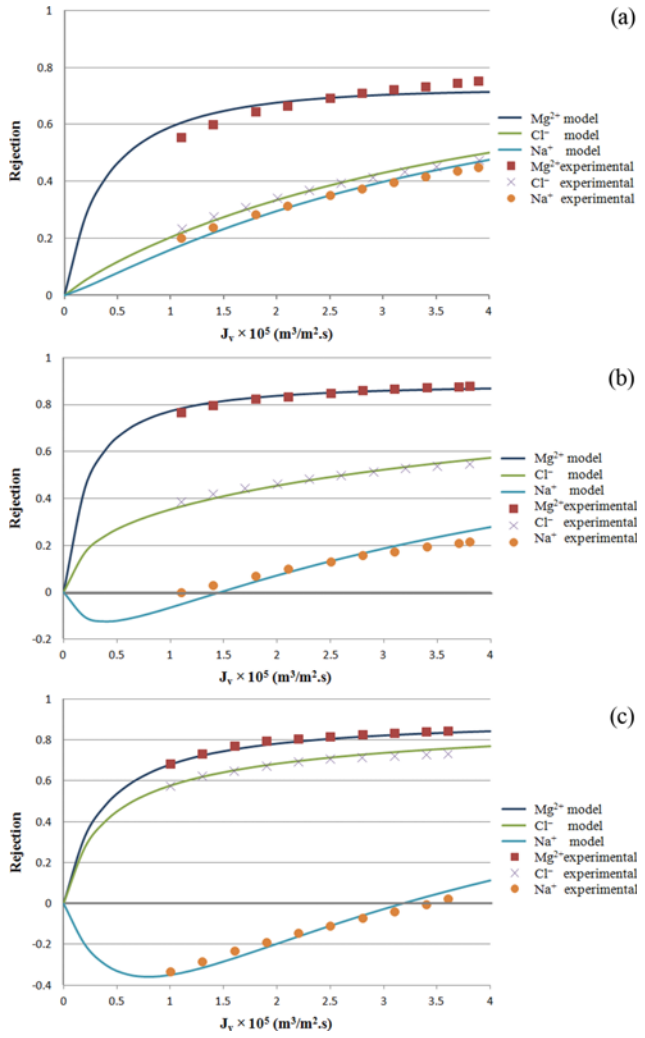

Fig. 6. Comparison between experimental data [8] and simulation at various molar ratios of NaCl/$MgCl_2$ of (a) 90/10 (b) 50/50 (c) 10/90.

the membrane (ε_p) is also decreased. The first one causes reduction in attracting forces of positive ions to negatively charged membrane, while the second one results in increasing dielectric exclusion effects (increasing rejection consequently).

In all cases, rising rejection at higher fluxes of permeate is observed for all components, as it was expected, due to more transportation of water molecules.

To compare components of this mixture and electrolyte solution of NaCl+Na_2SO_4, which is explained in the previous section, it is anticipated that the rejection of Mg^{2+} totally differs from that of SO_4^{2-}. This is due to the high positive charge density of Mg^{2+} that is attracted to the "negatively charged membrane" which results in a lower retention, in comparison with that of SO_4^{2-} (see Figs. 4 & 6). Based on Born equations (Eq. (31)), anions and cations have approximately similar dielectric exclusion (due to squared charge). Therefore, the rejection of Mg^{2+} would be relatively high, but less than rejection of SO_4^{2-}. This could be attributed to higher contribution of electrical exclusion relative to dielectric exclusion. From a different point of view, as said before that the divalent ions carry high charge density, they could affect the ionic strength of electrolyte as well as $\langle z_i \rangle$ which is usually a main coefficient unequal to unity for non-monovalent ions, precisely affecting the equations and the results, while Figs. 4 and 6 show good agreement for experimental and model prediction of Mg^{2+} and SO_4^{2-} respectively (Refer to claim #4.).

Concentration and electric potential distributions of the three ions in all three cases at a constant J_v(=2×10^{-5} $m^3/m^2 \cdot s$) are demonstrated in Fig. 7(a), (b), (c). In Fig. 7(a), concentration of Mg^{2+} inside the membrane is about zero (as a result of high rejection by membrane and low concentration in the feed side). By comparing Fig. 7(a) to 7(c), one can deduce that the concentration of Mg^{2+} is increased in the feed side, while the same is also increased in the membrane as well as in the permeate side. As discussed earlier, this matter motivates propagation of the gap between Na^+ and Cl^- ion concentrations in the permeate.

On the other hand, the concentration of Na^+ ions is decreased and that of Mg^{2+} ions is increased in the feed side conducting from Fig. 7(a) to 7(c). These three figures prove that increasing concentration of Mg^{2+} in the feed side will decrease rejection of Na^+ (change in the slope of concentration profile to positive value as evidence).

Despite the fact that some literatures [5,49] assume linear electric potential across the pore length, which imposes some simplifications, we have no particular considerations (with the exception of neglecting radial distribution for electric potential). Figs. 5 and 7 obviously reveal that the electric potential profile did not vary linearly, especially when the third species (divalent species) concentration increases. Therefore, such simplification may not be valid for many cases.

3. Comparison between GNP and GMS Models

Since the accuracy, which is introduced in Table 9, is somehow implying the goodness of fit while simultaneously plotting the simulated results from this manuscript and that of Déon, makes it very hard to distinguish between, we could suffice making the comparison through Q (of Déon introduced in Eq. (58)) and our accuracy.

Comparing these two parameters generally reveals the adequacy of Déon's model, although graphical comparison claims somewhere that Déon's model operates better and somewhere our GMS model. Since the number of fitted parameter is 2 vs. 3 (in our job), one may assert the Déon's model would be better, but with regards to being closer to real conditions (adsorption of ions to pore wall and employing Freundlich isotherm for varying membrane pore charge density), the authors certainly prefer the GMS model.

To some other extent, it is possible to compare the trend of changes of Q^* and X within our model and conventional Nernst-Planck, respectively. Since those parameters have not comparable values, it seems that plotting them for tree different solutions with primary and secondary axis would help comparing the trends (see Fig. 8(a) and 8(b)) between Déon's work and this work. The dashed lines point to the former and solid lines point to the latter.

Fig. 8(a) shows the dielectric constants of pores at same conditions (solutions, operational conditions, physical properties, *etc.*), while the solid line utilizes GMS and the dashed one employs GNP. Interestingly, not only the trends but also the values are in a good consistency within both mixture solutions. Also in Fig. 8(b) the membrane charge density (of GNP) on the left-hand side axis and

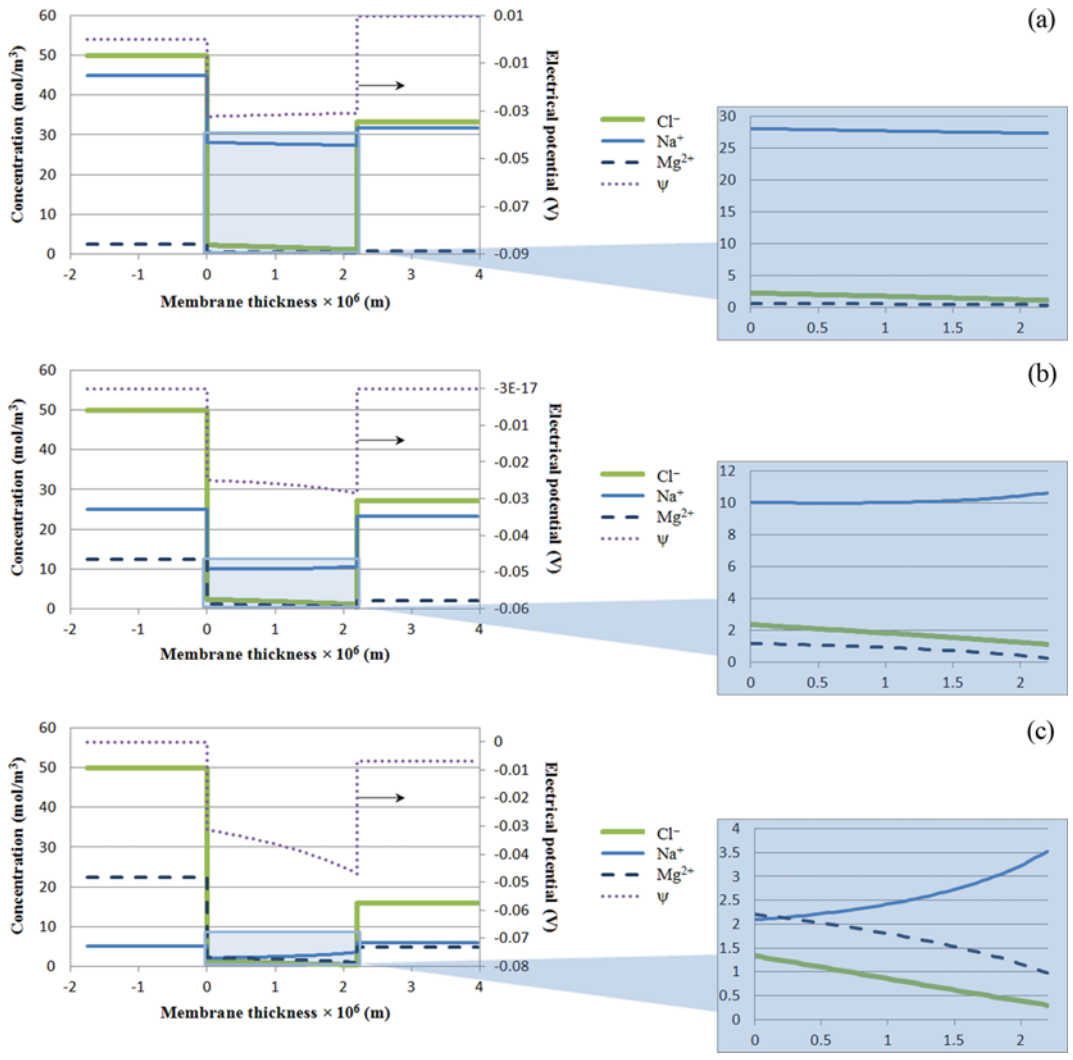

Fig. 7. Concentration and electric potential distribution at various molar ratios of $NaCl/MgCl_2$ of (a) 90/10 (b) 50/50 (c) 10/90.

$C_{tot}Q^*(\sum|z_i|x_i^{avr})^{K_s}$ (of GMS) on right-hand side axis are demonstrated. An acceptable similar trend for $NaCl+Na_2SO_4$ solution is observed, whereas that of $NaCl+MgCl_2$ solution is uncertainly incoherent. Anyhow, values of membrane charges on both vertical axes are approximately in good agreement. Of course, precursor outcome does not jeopardize the experimentally assessed results in the original study of Déon et al. [8]. The divergence may occur as different approaches for modeling as well as distinct method to describe the physical principle of membrane charge. This is probably related to adsorption of Mg^{2+} inside the pores which conforms to negatively charged membrane, which is considered in the current modeling.

CONCLUSIONS

The Maxwell-Stefan model was used to investigate the separation of mixed solutions of salts with common ion by NF. The aim was to test the ability of the GMS model to describe the separation of ions of greater complexity, *i.e.* containing three ions (four components since water is considered as solvent), generalization for N_c components and M mesh-grids in addition to considering non-ideality of electrolyte, dielectric exclusion, and non-uniform charge density along the pore simultaneously, by nanofiltration. A numerical model was developed to simulate the mass transfer of such multi-component electrolyte solutions through charged nanofiltration membranes, based on the Donnan steric partitioning pore, and dielectric exclusion model. The model incorporates the membrane micro structural parameters, the solute molecular properties, the feed solution physical properties and the operational conditions into one rigorous mathematical description. A unique approach was applied for the solution of equations, which was found to be capable in predicting the experimental data.

The predictions of the observed solute rejection coefficients agree well with the experimental and numerical values reported in the literature, for multi-ionic systems of $NaCl+Na_2SO_4$ and $NaCl+MgCl_2$ at three various concentrations for each system. The model can be used to describe the transport through pores of cylindrical geometries. The coupling among the various mechanisms involved in the retention phenomenon is pointed out and discussed. The volume charge density of an NF polyamide membrane was determined through a Freundlich type isotherm that relates mole fraction of

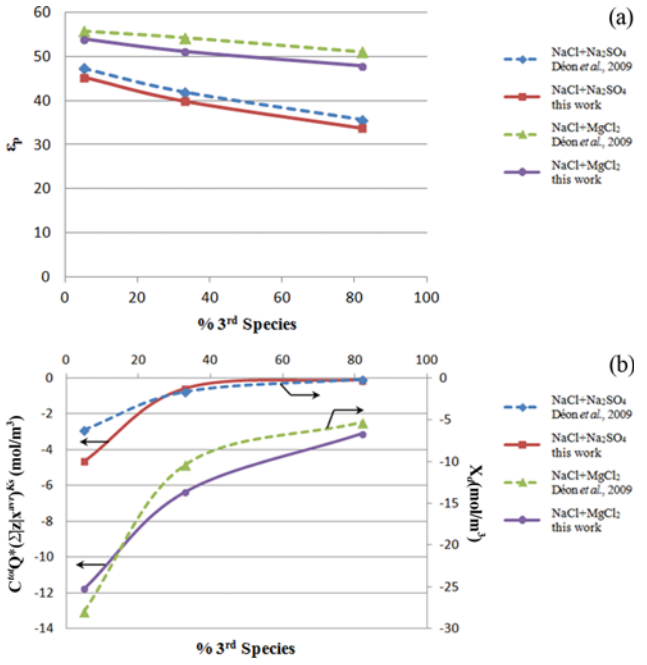

Fig. 8. Comparison between GNP and GMS models through (a) fitted pore dielectric constant (b) membrane charge density and Freundlich isotherm constant.

ions to the charge density of membrane. The model was then used to assess the rejection rate of the membrane, the dielectric constant of the solution filled the pores, Q^* and K_s as an adjustable parameter of the model. It is clearly shown that the dielectric exclusion cannot be neglected in the analysis of the filtration properties of NF membranes.

In the last section, two comparisons between i) dielectric constant of pores and ii) the trend of changes on $Q^*(\sum|z_i|x_i^{avr})^{K_s}$ and X (within our model and conventional Nernst-Planck respectively) were made. For the second one, results were plotted on one figure with primary and secondary axis to help making comparison. Results show the dielectric constants of pores at same conditions interestingly are in a good consistency (not only the trends but also the values) for both mixture solutions. The most important collation would be that for membrane charge density (of GNP) and $Q^*(\sum|z_i|x_i^{avr})^{K_s}$ (of GMS). Similar trend for NaCl+Na_2SO_4 solution was observed, whereas shallower analogy for NaCl+$MgCl_2$ solution could be attributed to adsorption of Mg^{2+} inside the pores, which is expected within negatively charged membrane.

ACKNOWLEDGEMENTS

The research council at Iran University of Science and Technology (IUST) as well as R&D department of National Iranian Gas Company (NIGC) is highly appreciated for their financial support during the course of this project.

NOMENCLATURE

A : cross sectional area of control volume [m^2]
B_0 : hydraulic permeability [m^2]
c : molar concentration inside membrane [mol/m^3]
C : molar concentration outside membrane [mol/m^3]
C_{tot} : total molar concentration [mol/m^3]
D_{ij} : diffusion coefficient [m^2/s]
$Đ_{i,k}$: Maxwell-Stefan diffusion coefficient [m^2/s]
F : Faraday constant (9.64867×10^4 C/eq)
$\mathscr{F}_i$: net driving force acting on component *i*
I_x : ionic strength [mol/*l*]
J_i : flux of component *i* [$mol/m^2{\cdot}s$]
k_B : Boltzmann constant (1.38066×10^{-23} J/K)
K_s : Freundlich parameter, (dimensionless)
L_{ij} : Onsager phenomenological coefficient
L_p : membrane permeability [$m^3/m^2{\cdot}s{\cdot}Pa$]
N_{avog} : Avogadro number, (6.023×10^{23} mol^{-1})
N_c : number of components
N_i : molar flux [$mol/m^2{\cdot}s$]
P : pressure [Pa]
Q^* : Freundlich parameters, (dimensionless)
R : ideal gas constant (8.314 J/mol·K)
r_i : stokes radius of ions [m]
r_p : average pore radius [m]
T : temperature [K]
u : average velocity [m/s]
u_i : diffusion velocity [m/s]
v_f : viscous velocity [m/s]
V_i : partial molar volume of ion *i* [m^3/mol]
w_i : net velocity of each component [m/s]
X : membrane charge density [mol/m^3]
x : mole fraction inside membrane
y : mole fraction outside membrane
z_i : charge number
0^+ : membrane-side interface
0^- : feed-side interface
<> : indicator of coefficient of variables in linearized form

Subscripts

+ : cation
− : anion
c : component
e : eastern control volume
exp : experimental
f : convective flow
i : component *i*
i, w : component *i* in water
i, m : component *i* in membrane
j : component *j*
k : component *k*
P : on-grid value or constant pressure
p : permeate or pore
s : solute
sim : simulated
T : at constant temperature
tot : total concentration
w : western control volume
avr : average value

Superscripts

* : value at previous iteration
° : at standard conditions

Greek Letters

α_i : viscous selectivity of component *i*
α_i' : bugger factor
δ : relaxation factor
ΔV : volume of control volume [m^3]
$\Delta W_{i,Born}$: Born salvation energy barrier [J]
Δy^+ : permeate-side interface
Δy^- : membrane-side interface
Δy : membrane thickness
δy : distance between two consecutive nodes [m]
ε : permittivity of the medium [F/m] or porosity of membrane
ε_0 : vacuum permittivity (8.854×10^{-12} F/m)
ε_b : bulk dielectric constant
ε_m : membrane material dielectric constant
ε_p : pore dielectric constant
φ : steric partitioning factor
γ : activity coefficient
η : dynamic viscosity [kg/m·s]
λ_i : ratio of solute *i* radius to pore radius
μ : chemical potential [J/mol]
Π : osmotic pressure [Pa]
ρ : density of fluid [m^3/s]
τ : tortuosity of the pores
ψ : electric potential [V]
ζ : friction coefficient

REFERENCES

1. R. W. Baker, J. G. Wijmans, A. L. Athayde, R. Daniels, J. H. Ly and M. Le, *J. Membr. Sci.*, **137**, 159 (1997).
2. W. R. Bowen and H. Mukhtar, *J. Membr. Sci.*, **112**, 263 (1996).
3. R. Levenstein, D. Hasson and R. Semiat, *J. Membr. Sci.*, **116**, 77 (1996).
4. W. R. Bowen, B. Cassey, P. Jones and D. L. Oatley, *J. Membr. Sci.*, **242**, 211 (2004).
5. W. R. Bowen, J. S. Welfoot and P. M. Williams, *AIChE J.*, **48**, 760 (2002).
6. W. R. Bowen and J. S. Welfoot, *Chem. Eng. Sci.*, **57**, 1121 (2002).
7. S. Déon, P. Dutournié and P. Bourseau, *AIChE J.*, **53**, 1952 (2007).
8. S. Déon, P. Dutournié, L. Limousy and P. Bourseau, *Sep. Purif. Technol.*, **69**, 225 (2009).
9. S. Déon, A. Escoda and P. Fievet, *Chem. Eng. Sci.*, **66**, 2823 (2011).
10. F. Fadaei, V. Hoshyargar, S. Shirazian and S. N. Ashrafizadeh, *Desalination*, **284**, 316 (2012).
11. F. Fadaei, S. Shirazian and S. N. Ashrafizadeh, *Desalination*, **281**, 325 (2011).
12. V. Geraldes and A. M. Brites Alves, *J. Membr. Sci.*, **321**, 172 (2008).
13. A. W. Mohammad, N. Hilal, H. Al-Zoubi and N. A. Darwish, *J. Membr. Sci.*, **289**, 40 (2007).
14. A. Szymczyk, N. Fatin-Rouge, P. Fievet, C. Ramseyer and A. Vidonne, *J. Membr. Sci.*, **287**, 102 (2007).
15. R. Krishna, *Chem. Eng. J.*, **35**, 19 (1987).
16. R. Krishna and J. A. Wesselingh, *Chem. Eng. Sci.*, **52**, 861 (1997).
17. J. A. Wesselingh and R. Krishna, *Mass transfer in multicomponent mixtures*, Delft University Delft, Netherland (2000).
18. R. Taylor and R. Krishna, *Multicomponent mass transfer*, Wiley (1993).
19. J. Mitrovic, *Int. J. Heat Mass Transfer*, **40**, 2373 (1997).
20. G. R. Gavalas, *Ind. Eng. Chem. Res.*, **47**, 5797 (2008).
21. S. Sircar and T. C. Golden, *Sep. Sci. Technol.*, **35**, 667 (2000).
22. R. Krishna and J. M. van Baten, *Ind. Eng. Chem. Res.*, **45**, 2084 (2006).
23. H. D. Do and D. D. Do, *Chem. Eng. Sci.*, **53**, 1239 (1998).
24. H. W. Hung, T. F. Lin, C. Baus, F. Sacher and H. J. Brauch, *Environ. Technol.*, **26**, 1371 (2005).
25. S. Li, V. A. Tuan, R. D. Noble and J. L. Falconer, *Environ. Sci. Technol.*, **37**, 4007 (2003).
26. J. A. Hogendoorn, A. J. van der Veen, J. H. G. van der Stegen, J. A. M. Kuipers and G. F. Versteeg, *Comput. Chem. Eng.*, **25**, 1251 (2001).
27. W. Lehnert, J. Meusinger and F. Thom, *J. Power Sources*, **87**, 57 (2000).
28. A. Runstedtler, *Chem. Eng. Sci.*, **61**, 5021 (2006).
29. K. Kaczmarski, A. Cavazzini, P. Szabelski, D. Zhou, X. Liu and G. Guiochon, *J. Chromatogr. A*, **962**, 57 (2002).
30. F. A. Banat, F. A. Al-Rub and M. Shannag, *Heat Mass Transfer*, **35**, 423 (1999).
31. H. C. No, H. S. Lim, J. Kim, C. Oh, L. Siefken and C. Davis, *Nuclear Eng. Design*, **237**, 997 (2007).
32. A. Szymczyk, P. Fievet and C. Ramseyer, *Desalination*, **200**, 125 (2006).
33. D. Vezzani and S. Bandini, *Desalination*, **149**, 477 (2002).
34. A. Szymczyk and P. Fievet, *Desalination*, **200**, 122 (2006).
35. A. E. Yaroshchuk, *Adv. Colloid Interface Sci.*, **85**, 193 (2000).
36. G. Bargeman, J. M. Vollenbroek, J. Straatsma, C. G. P. H. Schroën and R. M. Boom, *J. Membr. Sci.*, **247**, 11 (2005).
37. J. Straatsma, G. Bargeman, H. C. van der Horst and J. A. Wesselingh, *J. Membr. Sci.*, **198**, 273 (2002).
38. G. D. Mehta, T. F. Morse, E. A. Mason and M. H. Daneshpajooh, *J. Chem. Phys.*, **64**, 7 (1976).
39. T. R. Noordman and J. A. Wesselingh, *J. Membr. Sci.*, **210**, 227 (2002).
40. E. A. Mason and H. K. Lonsdale, *J. Membr. Sci.*, **51**, 1 (1990).
41. J. A. Wesselingh, P. Vonk and G. Kraaijeveld, *The Chemical Engineering J. and the Biochemical Engineering J.*, **57**, 75 (1995).
42. A. M. Lali, A. S. Khare, J. B. Joshi and K. D. P. Nigam, *Powder Technol.*, **57**, 39 (1989).
43. S. Patankar, *Numerical heat transfer and fluid flow*, CRC Press (1980).
44. S. Déon, P. Dutournié, P. Fievet, L. Limousy and P. Bourseau, *Water Res.*, **47**, 2260 (2013).
45. M. D. Afonso and M. N. de Pinho, *Ind. Eng. Chem. Res.*, **37**, 4118 (1998).
46. W. R. Bowen, A. W. Mohammad and N. Hilal, *J. Membr. Sci.*, **126**, 91 (1997).
47. J. Schaep, C. Vandecasteele, A. Wahab Mohammad and W. Richard Bowen, *Sep. Purif. Technol.*, **22-23**, 169 (2001).
48. S. Bandini and D. Vezzani, *Chem. Eng. Sci.*, **58**, 3303 (2003).

APPENDIX A: ENUMERATION VECTOR OF UNKNOWN VARIABLES

The [X] vector that represents unknown variables (refer to Fig. 3) is the basis for generalizing the evaluation and solving process. The corresponding matrix of coefficient [A], as well as [B] vector of constants can also be generated via same addressing no matter how much the number of components is (insert as the program input). Such vector is suggested to be generated in the form of:

One can count on this enumeration in generalization for components and grid-mesh as a part of solver fulfillment (due to addressing for each variable in general case of computer program). Such addressing would help to form generalized coefficients matrix [A] and constants vector [B], respectively.

$$
X=\begin{bmatrix}
\left.\begin{matrix} x_{11} \\ x_{21} \\ \vdots \\ x_{1p} \\ x_{2p} \end{matrix}\right\} (M+1)N_c \\
\left.\begin{matrix} \psi_1 \\ \psi_2 \\ \vdots \\ \psi_M \\ \psi_p \end{matrix}\right\} M+1 \\
\left.\begin{matrix} N_1 \\ \vdots \\ N_{N_c} \end{matrix}\right\} N_c \\
\left.\begin{matrix} P_1 \\ P_2 \\ \vdots \\ P_M \end{matrix}\right\} M
\end{bmatrix}
\begin{matrix}
\left.\begin{matrix} \\ \\ \\ \\ \\ \\ \\ \\ \\ \end{matrix}\right\} (M+1)(N_c+1) \\
\left.\begin{matrix} \\ \\ \\ \\ \\ \\ \\ \\ \\ \end{matrix}\right\} (M+2)(N_c+1)-1 \\
\left.\begin{matrix} \\ \\ \\ \\ \\ \\ \\ \\ \\ \end{matrix}\right\} (M+1)(N_c+2)+N_c-1
\end{matrix}
$$

Supporting Information

Mass transfer simulation of nanofiltration membranes for electrolyte solutions through generalized maxwell-stefan approach

Vahid Hoshyargar, Farzad Fadaei, and Seyed Nezameddin Ashrafizadeh†

Research Laboratory for Advanced Separation Processes, Department of Chemical Engineering,
Iran University of Science and Technology, Narmak, Tehran 16846-13114, Iran
(*Received 18 August 2014 • accepted 7 November 2014*)

PART A: SOLVING THE MODEL EQUATIONS

The governing equations are numerically solved to calculate the unknown variables including x_i, ψ, pressure profile inside the membrane, $x_{i,permeate}$, $\psi_{permeate}$, and molar flux of each component. The model equations consist of ordinary differential, partial differential, exponential, non-linear and algebraic equations. Simultaneous solution of the set of equations is possible by linearization of the system to deal with linear equations instead of complex set of equations. Linearization is carried out in this work by applying Taylor expansion for the following multi-variable function:

$$f(x, y)\cong f(x^*, y^*)+\left.\frac{\partial f}{\partial x}\right|_{x^*, y^*}\times(x-x^*)+\left.\frac{\partial f}{\partial y}\right|_{x^*, y^*}\times(y-y^*) \tag{A.1}$$

Superscript (*) represents the value of the assigned variable in previous iteration of solving loop. In each iteration, all of linearized equations are solved using a matrix of AX=B to find X. Here A is square matrix of coefficient, B is vector of constants, and X is the unknown vector. New values of unknown variables then update the matrix A and vector B.

The equations which need linearization include partitioning equation at feed-membrane interface, partitioning equation at membrane/permeate interface, and Maxwell-Stefan equation. Maxwell-Stefan equation should be solved along the membrane pore. Therefore, the pore has to be discretized using Finite Volume method.

The membrane pore is divided into M grids and 2 grids for 2 interfaces. A schematic representation of membrane compartment and discretization procedure is provided in Fig. 2. A number of M grids inside the membrane would generate M−1 control volumes. Maxwell-Stefan is applied as a mass transport model to each control volume. Applying finite volume from Eq. (GMS):

$$\begin{aligned}&-\int_{\Delta V}\frac{RT}{\gamma_i}\nabla x_i\cdot dV-\int_{\Delta V}x_i\left(V_i+\zeta_{i,m}\alpha_i'\frac{B_0}{\eta}\right)\nabla P\cdot dV\\&-\int_{\Delta V}x_i\left(z_i+\zeta_{i,m}\alpha_i'\frac{B_0C_{tot}}{\eta}\sum_k x_kz_k\right)F\frac{d\psi}{dy}\cdot dV\\&=\int_{\Delta V}\frac{1}{C_{tot}}\left[\sum_k\zeta_{i,k}\frac{\tau}{\varepsilon}(x_kN_i-x_iN_k)+\zeta_{i,m}\frac{\tau}{\varepsilon}N_i\right]\cdot dV\end{aligned} \tag{A.2}$$

As an example, the third integral would be calculated in this manner:

$$f=-\int_{\Delta V}x_i\left(z_i+\zeta_{i,m}\alpha_i'\frac{B_0C_{tot}}{\eta}\sum_k x_kz_k\right)F\frac{d\psi}{dy}\cdot dV \tag{A.3}$$

Each grid-dependence variable should be replaced by the average of its value in former and latter boundary, whilst the differentiation should be replaced by difference:

$$\begin{aligned}&f(x_i, x_k, \psi)\\&=-\frac{x_{i,j+1}+x_{i,j}}{2}\left(z_i+\zeta_{i,m}\alpha_i'\frac{B_0C_{tot}}{\eta}\sum_k\frac{x_{k,j+1}+x_{k,j}}{2}z_k\right)F\frac{\psi_{j+1}-\psi_j}{\delta y}\end{aligned} \tag{A.4}$$

Linearization of triple-variable nonlinear function is applied by using Taylor expansion:

$$\begin{aligned}g_k=x_ix_k\psi=&g_k(x_i^*, x_k^*, \psi^*)+(x_i-x_i^*)\left.\frac{dg_k}{dx_i}\right|_{x_i^*, x_k^*, \psi^*}\\&+(x_k-x_k^*)\left.\frac{dg_k}{dx_k}\right|_{x_i^*, x_k^*, \psi^*}+(\psi-\psi^*)\left.\frac{dg_k}{d\psi}\right|_{x_i^*, x_k^*, \psi^*}\end{aligned} \tag{A.5}$$

$$\begin{aligned}g_k=x_ix_k\psi&=x_i^*x_k^*\psi^*+(x_i-x_i^*)x_k^*\psi^*+(x_k-x_k^*)x_i^*\psi^*+(\psi-\psi^*)x_i^*x_k^*\\&=(x_k^*\psi^*)x_i+(x_i^*\psi^*)x_k+(x_i^*x_k^*)\psi-2x_i^*x_k^*\psi^*\end{aligned} \tag{A.6}$$

Therefore, the electrical term is rewritten as:

$$\begin{aligned}f=&-z_iF\frac{x_{i,j+1}+x_{i,j}}{2}\frac{\psi_{j+1}-\psi_j}{\delta y}-\left(\sum_k\Lambda_kg_k\left(\frac{x_{i,j+1}+x_{i,j}}{2}, \frac{x_{k,j+1}+x_{k,j}}{2}, \psi_{j+1}\right)\right.\\&\left.-\Lambda_kg_k\left(\frac{x_{i,j+1}+x_{i,j}}{2}, \frac{x_{k,j+1}+x_{k,j}}{2}, \psi_j\right)\right)\end{aligned} \tag{A.7}$$

where $\Lambda_k=\zeta_{i,m}\alpha_i'\frac{B_0C_{tot}}{\eta}z_kF$

or:

$$\begin{aligned}f=&-z_iF\frac{x_{i,j+1}+x_{i,j}}{2}\frac{\psi_{j+1}-\psi_j}{\delta y}\\&-\sum_k\left(\Lambda_k\frac{x_{k,j+1}^*+x_{k,j}^*}{2}\psi_{j+1}^*\right)\frac{x_{i,j+1}+x_{i,j}}{2}\\&+\left(\Lambda_k\frac{x_{i,j+1}^*+x_{i,j}^*}{2}\psi_{j+1}^*\right)\frac{x_{k,j+1}+x_{k,j}}{2}\\&+\left(\Lambda_k\frac{x_{i,j+1}^*+x_{i,j}^*}{2}\times\frac{x_{k,j+1}^*+x_{k,j}^*}{2}\right)\psi_{j+1}\end{aligned} \tag{A.8}$$

$$
\begin{aligned}
&-2\Lambda_k\frac{x^*_{i,j+1}+x^*_{i,j}}{2}\times\frac{x^*_{k,j+1}+x^*_{k,j}}{2}\psi^*_{j+1}\\
&+\sum_k\left(\Lambda_k\frac{x^*_{k,j+1}+x^*_{k,j}}{2}\psi^*_j\right)\frac{x_{i,j+1}+x_{i,j}}{2}\\
&+\left(\Lambda_k\frac{x^*_{i,j+1}+x^*_{i,j}}{2}\psi^*_j\right)\frac{x_{k,j+1}+x_{k,j}}{2}\\
&+\left(\Lambda_k\frac{x^*_{i,j+1}+x^*_{i,j}}{2}\times\frac{x^*_{k,j+1}+x^*_{k,j}}{2}\right)\psi_j\\
&-2\Lambda_k\frac{x^*_{i,j+1}+x^*_{i,j}}{2}\times\frac{x^*_{k,j+1}+x^*_{k,j}}{2}\psi^*_j
\end{aligned}
$$

That reforms to

$$
\begin{aligned}
f=&-\frac{z_iF}{2\delta y}(x^*_{i,j+1}+x^*_{i,j})(\psi_{j+1}-\psi_j)\\
&+(\psi^*_{j+1}-\psi^*_j)(x_{i,j+1}+x_{i,j}-(x^*_{i,j+1}+x^*_{i,j}))\\
&-\sum_k\left(\Lambda_k\frac{x^*_{k,j+1}+x^*_{k,j}}{2}(\psi^*_{j+1}-\psi^*_j)\right)\frac{x_{i,j+1}+x_{i,j}}{2}\\
&+\left(\Lambda_k\frac{x^*_{i,j+1}+x^*_{i,j}}{2}(\psi^*_{j+1}-\psi^*_j)\right)\frac{x_{k,j+1}+x_{k,j}}{2}\\
&+\sum_k\left(\Lambda_k\frac{x^*_{i,j+1}+x^*_{i,j}}{2}\times\frac{x^*_{k,j+1}+x^*_{k,j}}{2}\right)\psi_j\\
&-\left(\Lambda_k\frac{x^*_{i,j+1}+x^*_{i,j}}{2}\times\frac{x^*_{k,j+1}+x^*_{k,j}}{2}\right)\psi_{j+1}\\
&+\sum_k 2\Lambda_k\frac{x^*_{i,j+1}+x^*_{i,j}}{2}\times\frac{x^*_{k,j+1}+x^*_{k,j}}{2}(\psi^*_{j+1}-\psi^*_j)
\end{aligned}
\tag{A.9}
$$

In order to avoid more stiffness and complication during the numerical procedure, it is suggested that $\sum_k x_k z_k$ is replaced by $(\frac{-X}{C_{tot}})$ (electroneutrality in membrane) for an easier calculation:

$$
\begin{aligned}
&-\int_{\Delta V}\frac{RT}{\gamma_i}\nabla x_i\cdot dV-\int_{\Delta V}x_i\left(V_i+\zeta_{i,m}\alpha'\frac{B_0}{\eta}\right)\nabla P\cdot dV\\
&-\int_{\Delta V}x_i\left(z_i-\zeta_{i,m}\alpha'\frac{B_0X}{\eta}\right)F\nabla\psi\cdot dV\\
&=\int_{\Delta V}\frac{1}{C_{tot}}\left[\sum_k\zeta_{i,k}\frac{\tau}{\varepsilon}(x_kN_i-x_iN_k)+\zeta_{i,m}\frac{\tau}{\varepsilon}N_i\right]\cdot dV
\end{aligned}
\tag{A.10}
$$

If the solving process is converged, no problem occurs due to replacing few variables by * values, *i.e.* values gathered in the previous iteration, and is considered as constant values. So:

$$
\begin{aligned}
&-\int_{\Delta V}\frac{RT}{\gamma_i}\nabla x_i\cdot dV-\overbrace{\left(V_i+\zeta_{i,m}\alpha'\frac{B_0}{\eta}\right)}^{\theta_i}\int_{\Delta V}x_i\nabla P\cdot dV\\
&-\overbrace{F\left(z_i-\zeta_{i,m}\alpha'\frac{B_0X}{\eta}\right)}^{\beta_i}\int_{\Delta V}x_i\nabla\psi\cdot dV\\
&=\int_{\Delta V}\frac{1}{C_{tot}}\left[\sum_k\zeta_{i,k}\frac{\tau}{\varepsilon}(x_kN_i-x_iN_k)+\zeta_{i,m}\frac{\tau}{\varepsilon}N_i\right]\cdot dV
\end{aligned}
\tag{A.11}
$$

For the case of product of two variables (*e.g.*: $x_i\nabla P$ or $x_i\nabla\psi$), it can be linearized as:

$$
\begin{aligned}
f(x,y)=xy\Rightarrow f(x,y)&\cong x^*y^*+y^*(x-x^*)\\
&+x^*(y-y^*)=x^*y+y^*(x-x^*)
\end{aligned}
\tag{A.12}
$$

Substituting x and y with the main variables gives:

$$
f(x_i,\nabla\psi)=x_i\times\nabla\psi\cong x^*_i\nabla\psi+\nabla\psi^*(x_i-x^*_i)
\tag{A.13}
$$

Integration of the two last terms in the left hand side would give:

$$
\begin{aligned}
\int x_i\times\nabla\psi\cdot dV&\cong\int x^*_i\nabla\psi\cdot dV+\int\nabla\psi^*(x_i-x^*_i)\cdot dV\\
&=x^*_i((A\psi)_e-(A\psi)_w)+\nabla\psi^*(x_i-x^*_i)\Delta V
\end{aligned}
\tag{A.14}
$$

$$
\begin{aligned}
\int x_i\times\nabla P\cdot dV&\cong\int x^*_i\nabla P\cdot dV+\int\nabla P^*(x_i-x^*_i)\cdot dV\\
&=x^*_i((AP)_e-(AP)_w)+\nabla P^*(x_i-x^*_i)\Delta V
\end{aligned}
\tag{A.15}
$$

So:

$$
\begin{aligned}
&-\frac{RT}{\gamma_i}((Ax_i)_e-(Ax_i)_w)\\
&-\beta_i(x^*_i((A\psi)_e-(A\psi)_w)+\nabla\psi^*(x_i-x^*_i)\Delta V)\\
&-\theta_i(x^*_i((AP)_e-(AP)_w)+\nabla P^*(x_i-x^*_i)\Delta V)\\
&=\frac{1}{C_{tot}}\left[\sum_k\zeta_{i,k}\frac{\tau}{\varepsilon}(x_kN_i-x_iN_k)+\zeta_{i,m}\frac{\tau}{\varepsilon}N_i\right]\times dV
\end{aligned}
\tag{A.16}
$$

In one-dimensional case: $\Delta V=\delta y\times1\times1$; $A=1\times1$:

$$
\begin{aligned}
&-\frac{RT}{\gamma_i}((x_i)_e-(x_i)_w)\\
&-\beta_i((x^*_i)_P((\psi)_e-(\psi)_w)+\nabla\psi^*((x_i)_P-(x^*_i)_P)\delta y)\\
&-\theta_i((x^*_i)_P((P)_e-(P)_w)+\nabla P^*((x_i)_P-(x^*_i)_P)\delta y)\\
&=\frac{\tau}{\varepsilon}\frac{1}{C_{tot}}\left[\sum_k\zeta_{i,k}[(x^*_k)_PN_i+N^*_i((x_k)_P-(x^*_k)_P)\right.\\
&\left.-(x^*_i)_PN_k+N^*_k((x_i)_P-(x^*_i)_P)]+\zeta_{i,m}N_i\right]\times\delta y
\end{aligned}
\tag{A.17}
$$

Since $(x_i)_P$ is not an on-grid value (central variable on control volume), so it is replaced by $((x_i)_w+(x_i)_e)/2$ to be adjusted with unknown variables:

$$
\begin{aligned}
&-\frac{RT}{\gamma_i}((x_i)_e-(x_i)_w)\\
&-\beta_i\left(\frac{(x^*_i)_w+(x^*_i)_e}{2}((\psi)_e-(\psi)_w)\right.\\
&\left.+\nabla\psi^*\left(\frac{(x_i)_w+(x_i)_e}{2}-\frac{(x^*_i)_w+(x^*_i)_e}{2}\right)\delta y\right)\\
&-\theta_i\left(\frac{(x^*_i)_w+(x^*_i)_e}{2}((P)_e-(P)_w)\right.\\
&\left.+\nabla P^*\left(\frac{(x_i)_w+(x_i)_e}{2}-\frac{(x^*_i)_w+(x^*_i)_e}{2}\right)\delta y\right)\\
&=\frac{\tau}{\varepsilon}\frac{1}{C_{tot}}\left[\sum_k\zeta_{i,k}\left[\begin{array}{l}\frac{(x^*_k)_w+(x^*_k)_e}{2}N_i+N^*_i\times\\ \left(\frac{(x_k)_w+(x_k)_e}{2}-\frac{(x^*_k)_w+(x^*_k)_e}{2}\right)\\ -\frac{(x^*_i)_w+(x^*_i)_e}{2}N_k-N^*_k\times\\ \left(\frac{(x_i)_w+(x_i)_e}{2}-\frac{(x^*_i)_w+(x^*_i)_e}{2}\right)\end{array}\right]+\zeta_{i,m}N_i\right]\times\delta y
\end{aligned}
\tag{A.18}
$$

PART B: LINIEARIZATION FOR CHARGE BALANCE INSIDE THE MEMBRANE

Charge balance inside the membrane is:

$$\sum \langle z_i \rangle x_i + \frac{X}{C_{tot}} = 0 \tag{B.1}$$

where X is net charge per unit volume (charge density) in which X is related to mole fraction by isotherms such as:

$$\frac{X}{C_{tot}} = -Q^* \left(\sum |z_i| x_i\right)^{K_s} \tag{B.2}$$

Where Q^* and K_s are model parameters. With combining Eqs. (B.1) and (B.2) gives:

$$\sum_i \langle z_i \rangle x_i \overbrace{-Q^* \left(\sum_i |z_i| x_i\right)^{K_s}}^{f(x_i)\ i=1\ldots N_C} = 0 \tag{B.3}$$

$$\begin{aligned} f \cong f(x_i^*) + \sum_i (x_i - x_i^*) \left.\frac{df}{dx_i}\right|_{x_i^*} &= -Q^* \left(\sum_i |z_i| x_i^*\right)^{K_s} \\ -\sum_i \left((x_i - x_i^*) \times Q^* |z_i| K_S \left(\sum_i |z_k| x_k^*\right)^{K_s - 1} \right) & \end{aligned} \tag{B.4}$$

So charge balance would be rewritten in the form of:

$$\begin{aligned} &\sum_i \langle z_i \rangle x_i - Q^* \left(\sum_i |z_i| x_i^*\right)^{K_s} \\ &\quad -\sum_i \left((x_i - x_i^*) \times Q^* |z_i| K_S \left(\sum_k |z_k| x_k^*\right)^{K_s - 1} \right) = 0 \end{aligned} \tag{B.5}$$

$$\begin{aligned} &\sum_i \langle z_i \rangle x_i - \sum_i \left(x_i \times Q^* |z_i| K_S \left(\sum_k |z_k| x_k^*\right)^{K_s - 1} \right) \\ &\quad = Q^* \left(\sum_i |z_i| x_i^*\right)^{K_s} - \sum_i \left(x_i^* \times Q^* |z_i| K_S \left(\sum_k |z_k| x_k^*\right)^{K_s - 1} \right) \end{aligned} \tag{B.6}$$

$$\begin{aligned} &\sum_i \left\langle z_i - Q^* |z_i| K_S \left(\sum_k |z_k| x_k^*\right)^{K_s - 1} \right\rangle x_i = Q^* \left(\sum_i |z_i| x_i^*\right)^{K_s} \\ &\quad - \left(\sum_k |z_k| x_k^*\right)^{K_s - 1} \sum_i (x_i^* \times Q^* |z_i| K_S) \end{aligned} \tag{B.7}$$

$$\begin{aligned} &\sum_i \left\langle z_i - Q^* |z_i| K_S \left(\sum_k |z_k| x_k^*\right)^{K_s - 1} \right\rangle x_i = Q^* \left(\sum_i |z_i| x_i^*\right)^{K_s} \\ &\quad - Q^* K_S \left(\sum_k |z_k| x_k^*\right)^{K_s - 1} \sum_i (|z_i| x_i^*) \end{aligned} \tag{B.8}$$

$$\begin{aligned} &\sum_i \left\langle z_i - Q^* |z_i| K_S \left(\sum_k |z_k| x_k^*\right)^{K_s - 1} \right\rangle x_i = Q^* \left(\sum_i |z_i| x_i^*\right)^{K_s} \\ &\quad - Q^* K_S \left(\sum_k |z_k| x_k^*\right)^{K_s} \end{aligned} \tag{B.9}$$

$$\sum_i \left\langle z_i - Q^* |z_i| K_S \left(\sum_k |z_k| x_k^*\right)^{K_s - 1} \right\rangle x_i = Q^* \left(\sum_i |z_i| x_i^*\right)^{K_s} (1 - K_s) \tag{B.10}$$

PART C: SIMULATING STIFF CONDITIONS IN COMPARISON

As said through section 3, numerical testing in [10] shows that the major cause for the stiff behavior of such systems would be the difference of scales between the diffusion coefficients (*e.g.* $D_{Na^+} = 0.302 \times 10^{-9}$ m^2/s and $D_{Mg^{2+}} = 0.429 \times 10^{-11}$ m^2/s) inside the membrane, so the highly stiff system introduced in section 4.2 of [10] is simulated with our model. The simulating condition is: Na^+ (10 mol/m^3), Cl^- (50 mol/m^3) and Mg^{2+} (20 mol/m^3), at 298 K. The other simulated conditions are $J_v = 5.0 \times 10^{-5}$ m/s, $\Delta y = 2.5$ μm, $r_p = 0.40$ nm, $X = -30$ mol/m^3 and $\varepsilon_p = 60$. The concentration polarization was not taken into account and the activity coefficients were calculated using the Davies equation. The hydrodynamic radius and diffusivity of the magnesium ion used in the simulation were 0.35 nm and 0.707 $\times 10^{-9}$ m^2/s, respectively. The GMS model results in following figures which shows less than 1% deviation with similar figure (Fig. 4 of [10]) that shows our GMS model is capable of dealing with stiff systems.

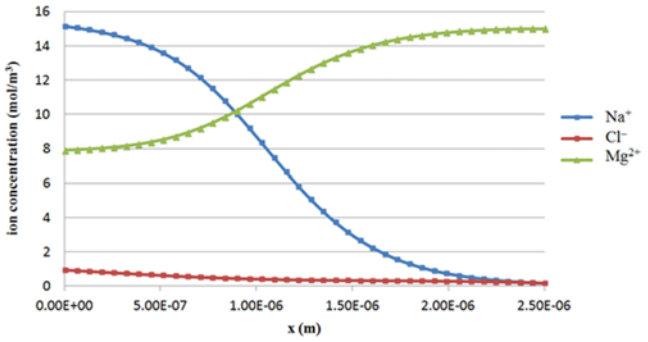

Fig. C.1. Ion concentration inside the membrane in a highly stiffed condition.

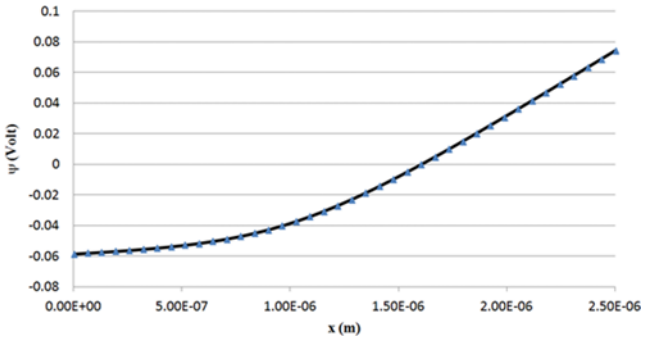

Fig. C.2. Electric potential inside the membrane in a highly stiffed condition.